https://doi.org/10.61092/iaea.vxnk-57m8

IAEA
International Atomic Energy Agency

INDC(NDS)-0815
Distr. G+NM+PH

INDC International Nuclear Data Committee

Photon Strength Functions in Thermal Neutron Capture II

Jiri Kopecky

JUKO Research

Alkmaar, The Netherlands

August 2020

IAEA Nuclear Data Section
Vienna International Centre, P.O. Box 100, 1400 Vienna, Austria

Selected INDC documents may be downloaded in electronic form
from *https://nds.iaea.org/publications*
or sent as an e-mail attachment.
Requests for hardcopy or e-mail transmittal should be directed to
NDS.Contact-Point@iaea.org
or to:
Nuclear Data Section
International Atomic Energy Agency
Vienna International Centre
PO Box 100
1400 Vienna
Austria

Printed by the IAEA in Austria

August 2020

INDC(NDS)-0815
Distr. G+NM+PH

Photon Strength Functions in Thermal Neutron Capture II

Jiri Kopecky

JUKO Research

Alkmaar, The Netherlands

August 2020

Table of Contents

Photon Strength Functions in Thermal Neutron Capture II

Introduction

Thermal capture data have been addressed in the 1st phase of this project [1] to test the results of the Photon Strength Functions (PSF) of thermal capture data. The choice of nuclides selected for the study was predominantly on targets with low and medium masses (A < 160) for two reasons. Firstly, the knowledge of the PSF behavior for medium and heavy mass targets had already been successfully addressed by a series of ARC and DRC experiments [2]. For targets bellow A~100, however, the lower-level density increases the possibility to detect primary transitions in a broad E_γ-range down to very low energies. In such cases, additional information on the E1 and- M1 strength in the 0 – 5 MeV energy range may be obtained, especially relevant for M1 strength behavior bellow the spin-flip resonance. Finally, in low mass targets the competition of the non-statistical and statistical models may be observed. The properties of the studied nuclides have been processed in the pilot data base ATLAS_f(L)_THC and includes 30 nuclides from ^{20}F up to ^{154}Eu and the derived PSF results were discussed in Ref. [1].

1. General observations

The main observation can be summarized as follows: the two-channel spin admixture in the capture state results in effects which do not exceed the general uncertainty of the PSF data, primarily originating from the Porter-Thomas and statistical fluctuations. This, to some extend is a surprising conclusion, and is based on a comparison of the systematic prediction from the DRC and THC data. The general data trend of the high energy data is almost the same as the DRC systematic for the data at the mean energy $E_\gamma = <6.5 \pm 0.5>$ MeV, which is demonstrated in Fig. 1 taken from Ref. [1].

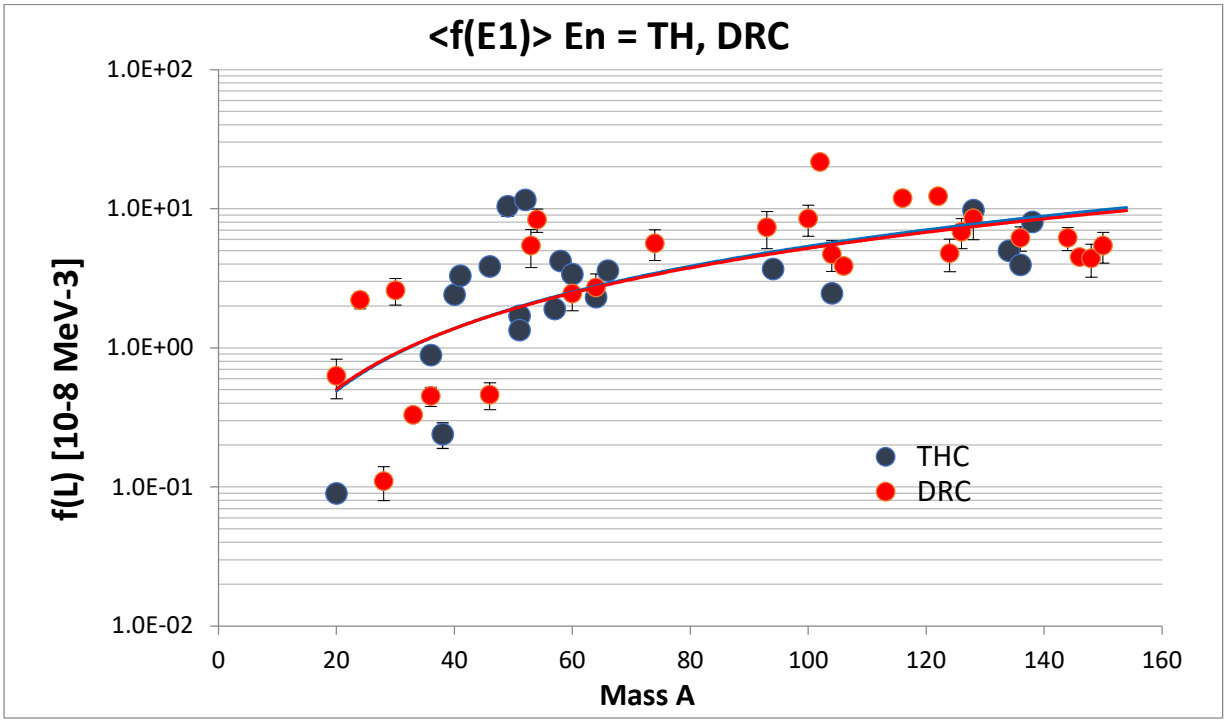

Fig.1 *Binned <f(E1)> values from THC and DRC experiments are plotted for nuclides with E1 transitions in the (6.5 ± 0.5) MeV energy window. Note the larger spread of the THC data for light nuclides with A < 60*

However, the comparison with theoretical predictions of the QPRA calculations (kindly provided by S. Goriely as a private communication; all details can be found in Ref. [3]) and shown in Fig. 2, reveal a rather strong strength enhancement at the lower gamma-ray energies, which is difficult to reconcile with the statistical compound nucleus theory. Examples of this enhancement are found for both E1 and M1 data for some light nuclei (^{19}F, ^{24}Na, ^{28}Al) and heavier targets (^{40}K and ^{52}V). Note the large strength found in ^{32}P and ^{58}Fe for E1 data and the M1 strength in ^{66}Cu, ^{94}Nb, ^{128}I and ^{136}Ba targets.

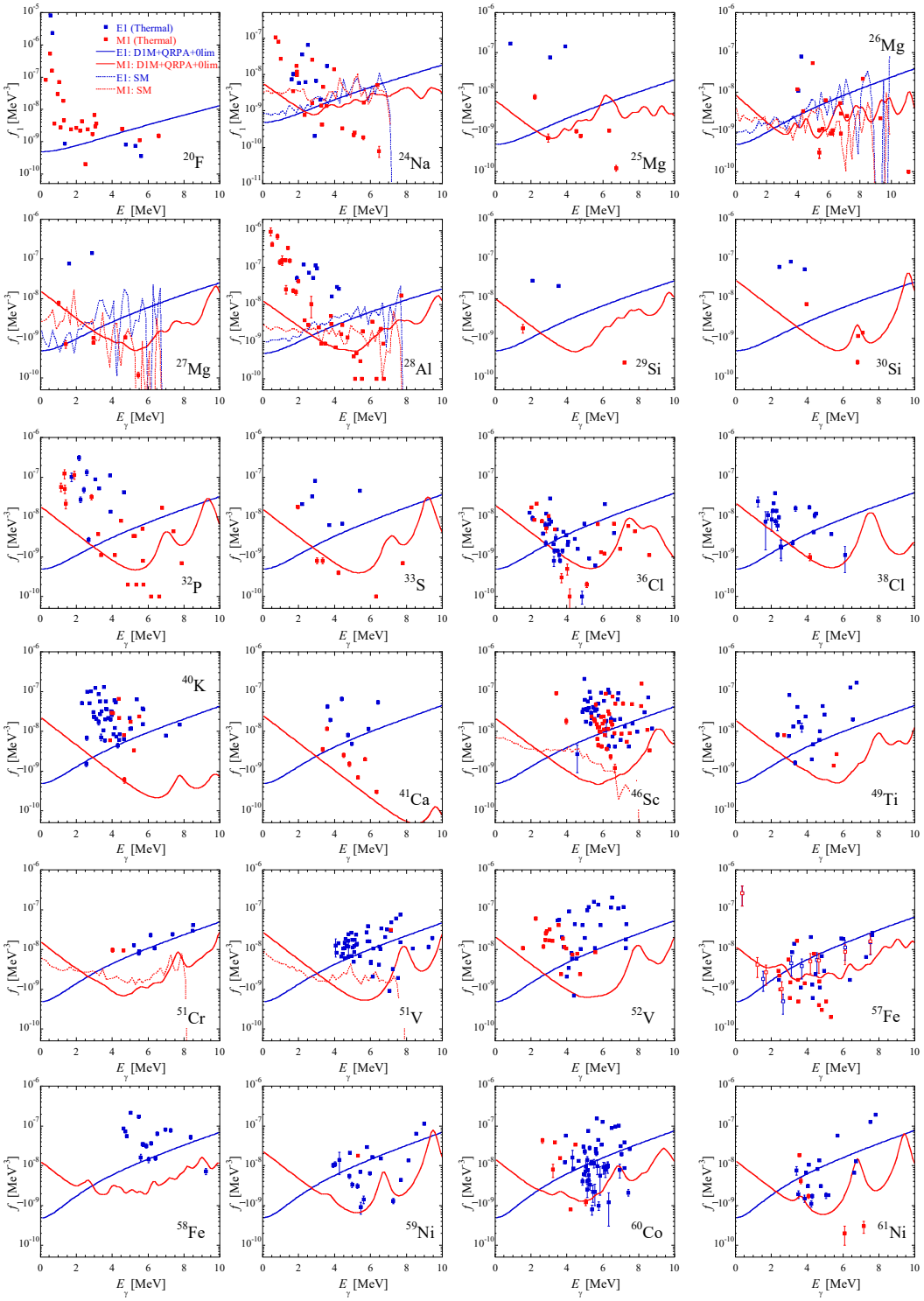
E1 (Thermal)
M1 (Thermal)
E1: D1M+QRPA+0lim
M1: D1M+QRPA+0lim
E1: SM
M1: SM
f_1 [MeV^{-3}]
E_γ [MeV]
^{20}F
^{24}Na
^{25}Mg
^{26}Mg
^{27}Mg
^{28}Al
^{29}Si
^{30}Si
^{32}P
^{33}S
^{36}Cl
^{38}Cl
^{40}K
^{41}Ca
^{46}Sc
^{49}Ti
^{51}Cr
^{51}V
^{52}V
^{57}Fe
^{58}Fe
^{59}Ni
^{60}Co
^{61}Ni

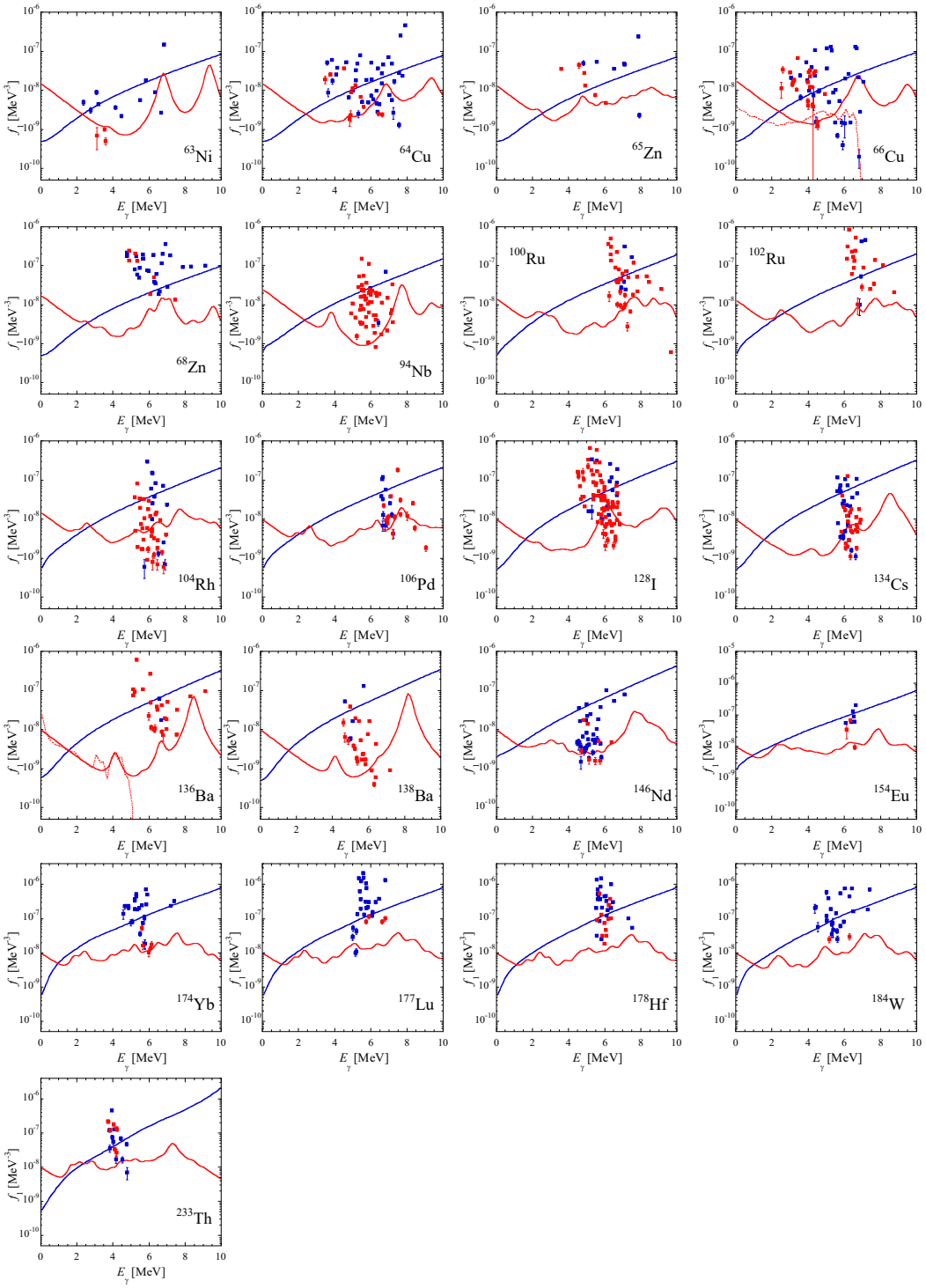

Fig.2 *Comparison of THC E1 and M1 strength from the Atlas_THC_f(L) database with the D1M+QRPA calculations (solid lines) [35]. In a few cases the shell model (SM; dotted lines) predictions at low energies are also given [3].*

Such effects, which are not in accord with the compound nucleus model, had been noticed in the early sixties and led Lane and Lynn to formulate the direct capture theory for E1 transitions

[4]. This model divides the capture in to the external (non-resonance) and internal (resonance) components. If the internal component is small or absent, the external direct (potential) capture is responsible for the cross section, which at thermal energies is primarily contributed by the incident 3s-wave to 2p-orbital single-particle E1 transitions. However, the presence or lack of corresponding orbits in other words, the final states, complicate this mechanism. We have, therefore, decided to review all earlier evidence on the non-statistical models and to add recent general results, in order to better understand the mentioned enhancement observation.

2. General remarks on E1 enhanced transitions

2 .1 Direct capture of Lane-Lynn for E1 transitions

The thermal cross section σ(th) is for many light mass nuclides usually low (< 1b). Such low cross section is typical for an off-resonance energy region, and direct-capture (mainly potential) is typically applicable for E1 transitions. The theoretical derivation for such transitions can be found in the original work of Lane and Lynn [4] and many other publications by Mughabghab or Raman as the main authors [5-14].

If the capture state is far away from resonances, the simplified non-resonant capture cross section $\sigma(\gamma)$ can be derived from the general relationship (Eq. (4) in Ref. [4]) in a form as

$$\sigma_\gamma = \Sigma_s\, \sigma_\gamma\,(hs)\ \{1 + \sigma_\gamma\,(dl)^2\}, \qquad (1)$$

where the hard sphere (elastic or potential) component is

$$\sigma_\gamma\,(hs) = 0.062/\sqrt{R}\ (Z/A)^2\ (2Jf + 1/6(2I + 1))\ S_n\ \{(y + 3)^2/(y - 1)^2\}\ y^2, \qquad (2)$$

and the distant levels (inelastic or valence) contribution from the wings of resonant scattering

$$\sigma_\gamma\,(dl) = [(R - a_s)/R]\ [y\ (y + 2)/y + 3], \qquad (3)$$

and E_γ dependent parameter $y^2 = R^2(2mE_\gamma)/h^2$; the subscript 's' indicates the two channel spins for $(I \pm ½)$.

The parameters in Eqs. (1-3) are described in Ref. [4], the relevant parameters for the present discussion are the radius of the sphere R (assumed to be approximately equal to the nuclear radius), the crucial coherent scattering length of thermal neutrons a_s and the (d,p) spectroscopic factor S_{dp}. The term $(R - a_s)$ determines the size of the distant levels contribution and if its value is small or equal to zero, the remaining hard sphere capture dominates the cross section and the cross-section is directly related to the $(2J_f + 1)\ S_n$ parameter, which represents the fractional content of the appropriate single particle mode of the p-orbital.

The Lane – Lynn theory was verified for several nuclei, the calculated partial transition cross-sections were successfully compared with the theoretical predictions, see Refs. [5-14]. The calculated data base of DC thermal cross-sections was included in Ref. [14] as one of the thermal cross-section parameters, as the experimental value σ(th) and the derived values σ(-),

σ(+), σ(B) and σ(D). The direct capture cross-section was calculated using Eqs. (1-3) and the resulting values are shown in Fig. 3, plotted as a function of the mass A.

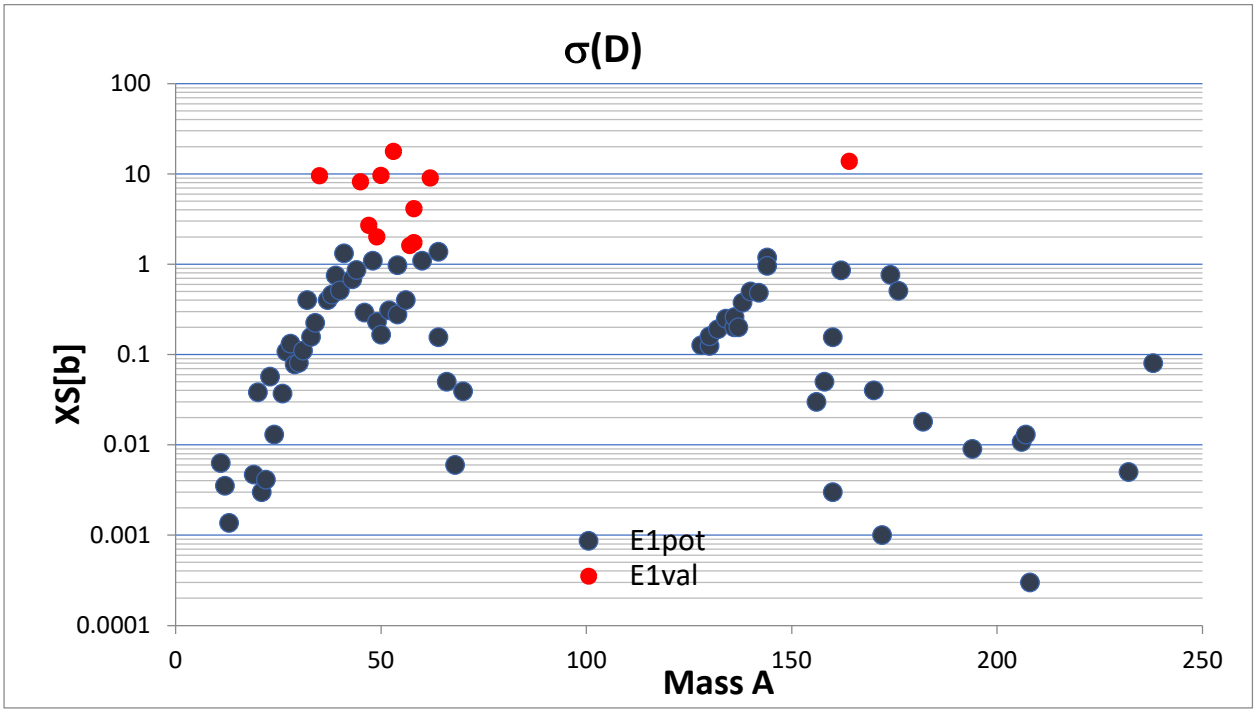

Fig.3 *Direct capture cross sections (better non-statistical) calculated with the Lane-Lynn formula from the cross-section compilation of Mughabghab [14]. Two giant s-resonances are present, the (3s – 2p) transitions around A = 50 and (4s -3p) close to A = 150. In these regions are present the E1 non-statistical processes. The red data points suggest the possible presence of the distant level (valence) capture component.*

2 .2 The (nγ)(dp) correlations as a signature of the E1 direct capture

This approach to the direct capture formulation was introduced by Kopecky and Spits (RCN Petten). They have followed the correlation between the reduced I_γ strength and the (d,p) striping factor $(2Jf+1)S_n$, the dependence of which is predicted by the σ_γ(hs) formula. The novel idea was to introduce the correlation exponent L of the E_γ^L reduction as a variable. The idea was not theoretically based but was a pure phenomenological trial. The first results were published in Refs. [16–21] and as a most illustrative example are the ^{38}Cl data shown in Fig. 4. The ^{38}Cl nucleus is a very suitable test case, because the thermal capture decay is due to E1 transitions and no multipolarity uncertainty in the data is present. Kopecky has generated a complete data base of (ng)(dp) correlation coefficients for nuclides with A < 70 Ref. [22], varying the reduction Eγ exponential factor L from 0 to 8. The linear correlation curve for ^{38}Cl clearly demonstrates the maximal correlation at L about one. This observation inspired Lane to include this feature in the Lane-Lynn model as a singularity effect and this was published in Ref. [23].

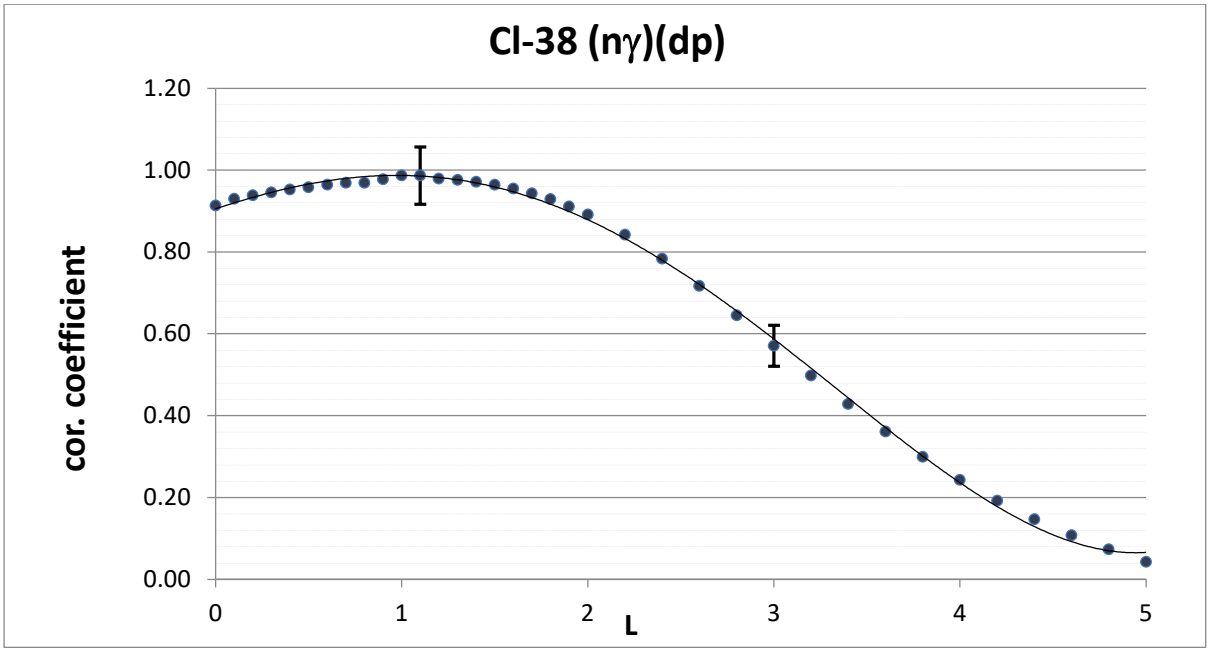

Fig.4 *The linear correlation coefficient between the reduced I_γ^L strength and the (d,p) spectroscopic factor $(2J_f+1)S_n$ of the ^{38}Cl nucleus, taken from Ref. [17,23], as a function of the exponent L showing a significant singularity .The values at L=3 and the L_{max}~1.0 are marked by the error bars.*

A similar example of this approach has been later made by Mughabghab when explaining the gamma ray strength in the ^{137}Xe nucleus and will be discussed in the Section 2.7. The major enhancement of the γ-ray strength in the THC data compared to the statistical predictions is present for data with A < 70, and we shall therefore concentrate in detail on this mass region.

2.3 Properties of the thermal capture for A < 70 (3s -> 2p region)

In order to get an overview which cross section component is dominating at the thermal energy, the list of cross section components for all stable nuclei below A < 70 was taken from Ref. [14] and is shown in Table 1. The relevant capture-state parameters are estimated from the positive (negative) resonance contributions. In the s-wave capture (dominant at thermal energies) the overlap of resonance tails generally results in an admixture α of two resonance spin states (see Ref. [1]).

The resonance contributions can be estimated from the resonance parameters and measured thermal cross sections. The contribution from resonances with positive energy above the binding energy can be estimated using the following equations:

$$\sigma(th) = \sigma(res) + \sigma(B) \qquad (4)$$

and $\sigma(res) = \sigma(-) + \sigma(+)$. (5)

The resonant contributions $\sigma(-)$ or $\sigma(+)$ originate from the positive s-wave resonances with J_t - 1/2 or J_t+1/2 spins, respectively and $\sigma(B)$ stands for the missing cross section from either bound-states (rarely determined) or non-resonant contributions of a non-statistical origin. The value of $\sigma(B)$ therefore represents the sum of negative resonance contributions and the nonstatistical (mainly direct) components.

Table 1. Thermal cross section parameters of stable nuclides with mass A < 70 taken from Ref. [14]. Important results are given in columns 4, 6 and 8. They indicate fractions of positive resonance contributions, bound state contributions and the direct capture to the bound state component. The grey shaded nuclides are not included in the recent ATLAS_THC_f(L) data base. The possibly dominant resonance or distant levels capture is indicated in bold for assumed $\sigma(D) > 1.5$ b value. No $\sigma(D)$ value reflects no data in Ref. [14].

Target	**$\sigma(\gamma)_0$**	**$\sigma(+) + \sigma(-) = \sigma(res)$**	**$\sigma(res) / \sigma(\gamma)_0$**	**$\sigma(B)$**	**$\sigma(B)/\sigma(\gamma)_0$**	**$\sigma(D)$**	**$\sigma(D)/\sigma(\gamma)_0$**
	[b]	[b]		[b]		[b]	
B-10	0.394	0.09	0.22				
B-11	0.009		0	0.009	1	0.0063	0.70
C-12	0.00387		0	0.0005	0.14	0.00353	0.91
C-13	0.00150	0.0015^+	1			0.00137	0.91
N-14	0.080	0.00851	0.10	0.007925	0.10		
N-15	0.00024	0.0000083	0.35	0.0000157	0.07		
O-16	0.000173	0.00005	0.27	0.000126	0.73	0.000183	1.06
O-17	0.00054		0	0.00054	1	0.00038	0.70
O-18	0.00015		0	0.000149	1	0.0001	0.67
F-19	0.0095	0.0029	0.31	0.0065	0.69	0.0047	0.50
Ne-20	0.037	0.0064	0.17	0.0306	0.83	0.0382	0.103
Ne-21	0.666		0	0.666	1	0.003	4e-4
Ne-22	0.0527	0.0098	0.19	0.04287	0.81	0.0041	0.08
Na-23	0.525	0.5129	0.98	0.012	0.02	0.057	1.06
Mg-24	0.0538	0.0022	0.09	0.0516	0.96	0.013	0.24
Mg-25	0.199	0.199	1		0		
Mg-26	0.0374		0	0.0374	1	0.037	1
Al-27	0.231	0.101	0.44	0.130	0.56	0.108	0.47
Si-28	0.177	0.0485	0.27	0.1285	0.73	0.132	0.75
Si-29	0.119	0.0017	0.01	0.1173	0.99	0.078	0.66
Si-30	0.107	0.0034	0.03	0.1036	0.97	0.081	0.76
P-31	0.166	0.0015	0.01	0.1615	0.97	0.110	0.66
S-32	0.518	0.084	0.16	0.434	0.84	0.401	0.77
S-33	0.454	0.004	0.009	0.450	0.99	0.157	0.36
S-34	0.256	0.0025	0.01	0.2535	0.99	0.224	0.88
Cl-35	43.6	0.067	0.002	43.6	1		
Cl-37	0.433	0.092	0.21	0.400	0.92	0.400	0.92
Ar-36	5.2		0	5.2	1	**9.54**	1.83
Ar-38	0.8		0		0	0.46	0.56

Ar-40	0.66	0.028	0.04	0.632	0.96	0.514	0.78
K-39	2.1	0.02	0.01	2.08	0.99	0.753	0.36
K-41	1.46	0.357	0.24	1.355	0.76	1.32	0.10
Ca-40	0.41	0.019	0.05	0.391	0.95	0.230	0.56
Ca-42	0.680	0.041	0.06	0.639	0.94	0.680	1
Ca-43	6.2	4.59	0.74	1.61	0.26		
Ca-44	0.88	0.053	0.06		0	0.865	0.98
Ca-48	1.09		0	1.09	1	1.09	1
Sc-45	27.2	0.89	0.03	26.33	0.97	**8.18**	0.30
Ti-46	0.59	0.10	0.06	0.49	0.83	0.292	0.49
Ti-47	1.63	0.89	0.55	0.74	0.45	**2.7**	1.66
Ti-48	8.32	4.1	0.49	4.22	0.51		
Ti-49	1.87	0.43	0.23	1.44	0.77	**2.01**	1.07
Ti-50	0.179	0.006	0.03	0.173	0.97	0.166	0.93
V-50	45	12.7	0.28	32.3	0.72		
V-51	4.94	3.62	0.73	1.32	0.27		
Cr-50	14.7	9.34	0.64	5.36	0.38	**9.6**	0.65
Cr-52	0.86	0.07	0.08	0.79	0.93	0.31	0.31
Cr-53	18.6	9.36	0.50	9.15	0.50	**17.8**	0.96
Cr-54	0.41	0.035	0.09	0.375	0.91	0.278	0.68
Mn-55	13.36	10.03	0.75	3.32	0.25		
Fe-54	2.30	1.49	0.65	0.81	0.35	0.98	0.43
Fe-56	2.59	0.09	0.03	2.50	0.97	0.40	0.15
Fe-57	2.48	1.14	0.46	1.34	0.55	**1.61**	0.65
Fe-58	1.32	0.21	0.16	1.11	0.84	**1.74**	1.32
Co-59	37.18	29.56	0.80	7.62	0.21		
Ni-58	4.39	0.32	0.07	4.07	0.93	**4.11**	0.94
Ni-60	2.45	1.44	0.59	1.01	0.41	1.09	0.45
Ni-62	14.9	14.9	1		0	**9.05**	0.61
Ni-64	1.63	0.72	0.44	0.91	0.56	1.37	0.84
Cu-63	4.50	0.433	0.10	4.097	0.91		
Cu-65	2.17	0.15	0.07	2.020	0.93		
Zn-64	0.731	0.559	0.77	0.172	0.23	0.155	0.21
Zn-66	0.62	0.227	0.37	0.393	0.63	0.050	0.08
Zn-67	7.5	3.65	0.49	3.85	0.51		
Zn-68	1.07	0.97	0.91	0.10	0.90	0.006	0.006
Zn-70	0.092	0.092	1		0	0.039	0.42

Two important conclusions can be derived from the Table 1. The thermal cross section for majority of is nuclides formed by the σ(B) component and not by the tails of positive resonances. The latter contribution forms only a few percent of the thermal cross section and is nicely shown in left-hand part of Fig. 5. The right-hand part of Fig.5 displays the share of the direct capture component in the σ(B) value. The direct (potential) capture for targets up to A = 50 is almost fully responsible for the σ(B) thermal cross section, while for A > 50 targets the distant levels valence and resonance capture start to play the dominant role. The direct capture pert starts to disappear at masses A ≥ 70 and the statistical compound process becomes

completely dominant. One of the reasons of the DC decrease may also be the decreased availability of the final p-states.

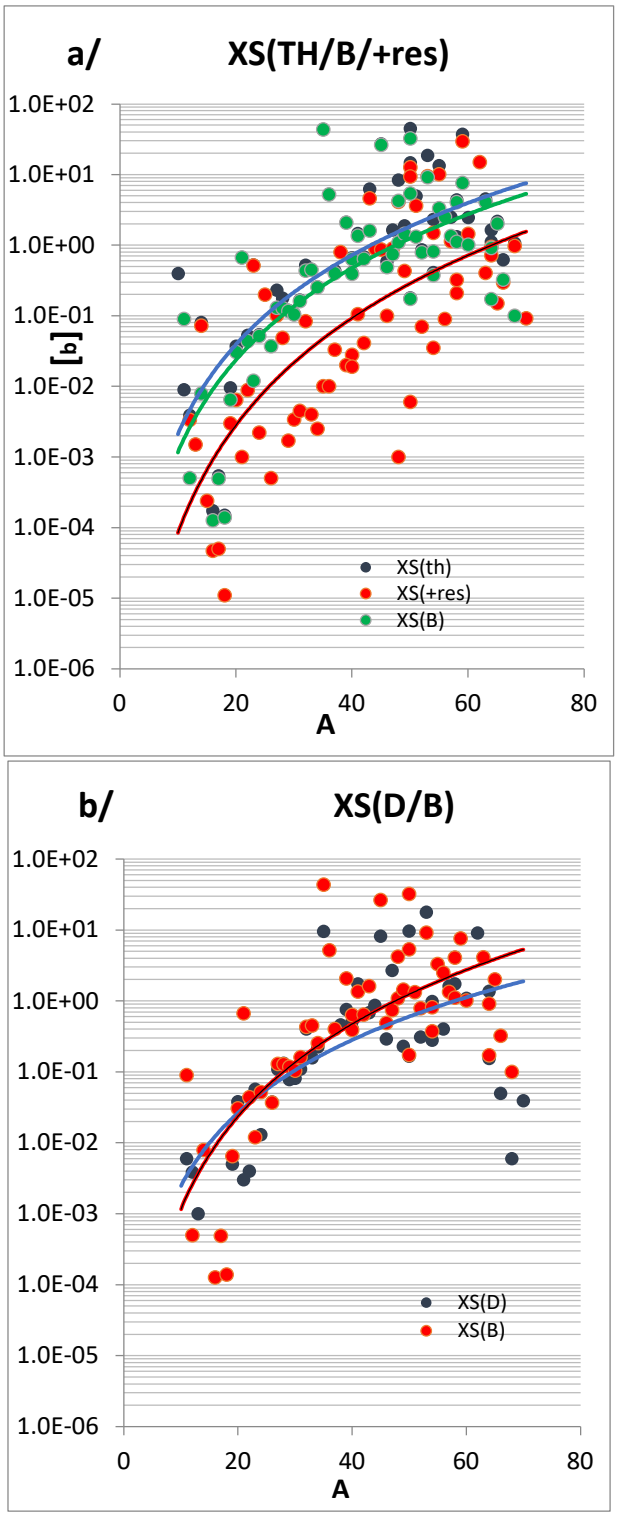

Fig. 5 *The extracted partial cross-*sections *σ(th), σ(res)= σ(-) + σ(+) and σ(B) for all stable targets with A < 70 are plotted in the left-hand part of the figure as a function of A, while the right-hand one shows the derived σ(B) and the calculated σ(D)values. Note the dominance of σ(B) against other contributions and the almost equality of σ(B) and σ(D), especially for masses with A < 50. All shown curves are the power trendlines of A.*

2.4 Thermal capture models for A < 70

The E1 non-statistical models have been nicely surveyed by Mughabghab in Ref. [25] from 1979. For a discrete resonance initial state *i* and final state *f*, the total radiative amplitude has been postulated as the sum

$$\Gamma_\gamma(\mathrm{if})^{1/2} = C_1\,\Gamma_\gamma(\mathrm{if})^{1/2}(\mathrm{sp}) + C_2\,\Gamma_\gamma(\mathrm{if})^{1/2}(\mathrm{ds}) + C_3\,\Gamma_\gamma(\mathrm{if})^{1/2}(\mathrm{cn}) \qquad (6)$$

where the contributions on the right-hand side are due to single particle, doorway state and compound nucleus processes. The constants C_i vary with the data mass regions and for masses greater than 150 the compound nucleus term is dominant. It seems reasonable to accept a similar summing of different reaction modes for the thermal capture cross section, keeping in mind that interference effects are also present. However, we have shown in Ref. [1], that the sum of partial cross sections is not severely influenced by these effects.

The calculated direct capture cross section for this mass region is shown in Fig. 6.

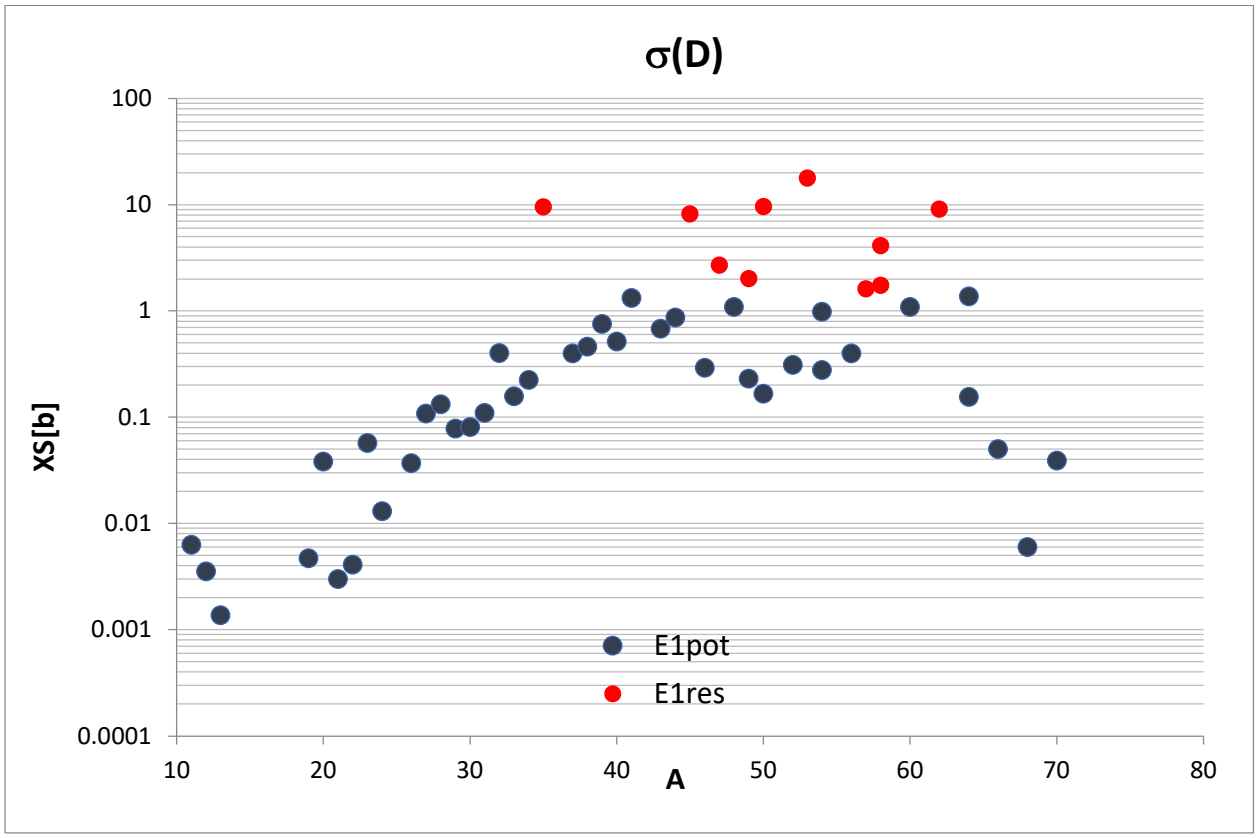

Fig.6 *The direct capture cross sections, calculated with the Lane-Lynn formula for the (3s – 2p) transitions in Ref. [14] is plotted as a function of the mass. The blue data points represent the hard-sphere potential direct capture, while the red points indicate the contribution of the distant levels or resonance components.*

The different reaction mechanisms for targets between 27 < A <66 were classified in Refs. [22,25], using the (nγ)(dp) correlation analysis and are graphically represented in two plots in Fig. 7 (Figs. 2 and 21 from Refs. [22, 25]). The mass region below A = 70 is divided in two parts, in which the non-statistical processes as direct and valence capture are dominant (Eq (2) + Eq. (3)) and slowly entering the statistical region for A > 60. It is important to remember, that the size of the valence process contribution is dependent on the $(R - a_s)/R$ term and varies from nucleus to nucleus.

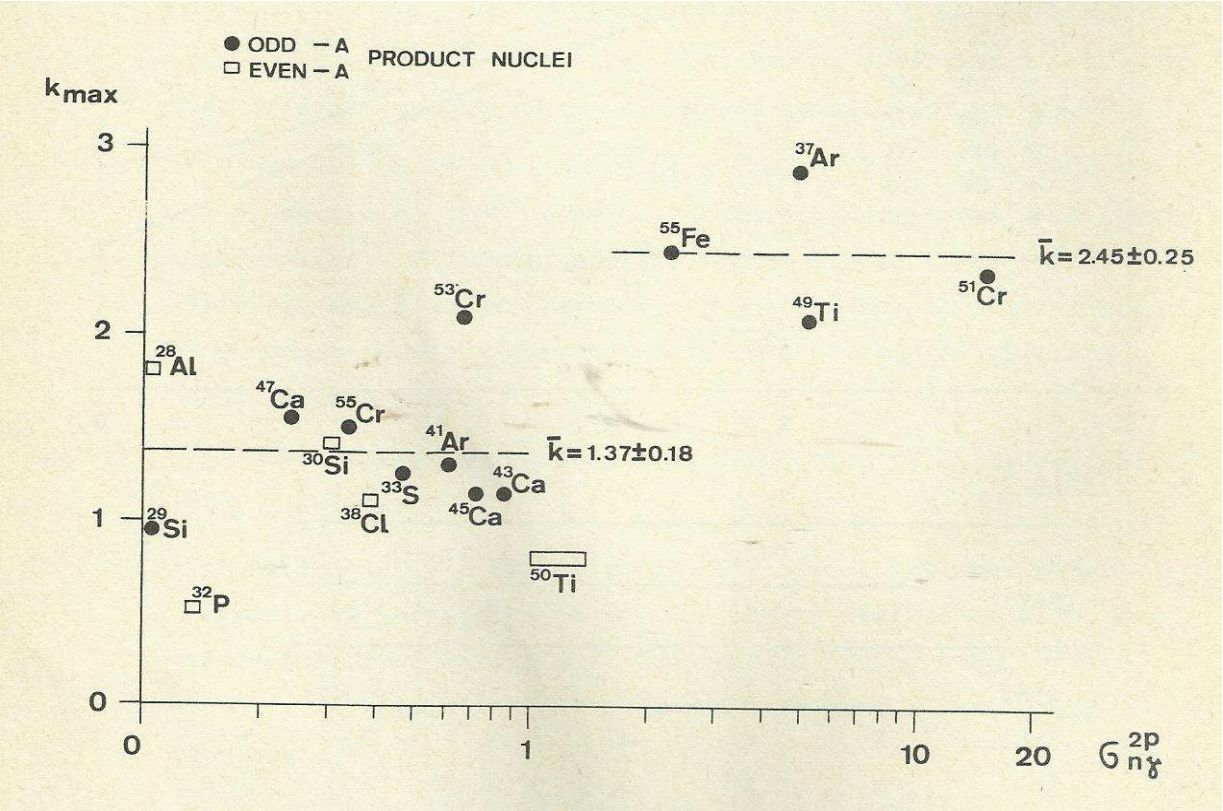

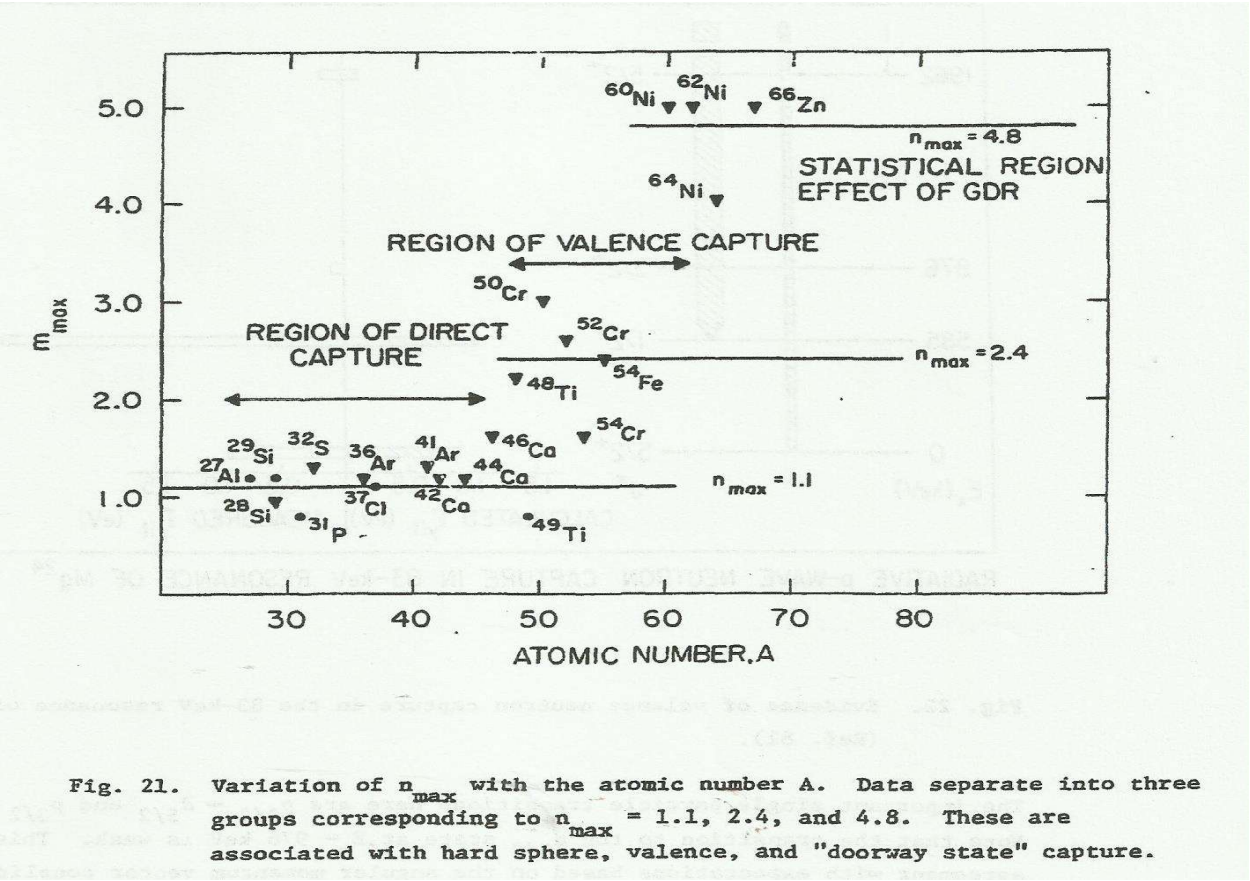

Fig. 21. Variation of n_{max} with the atomic number A. Data separate into three groups corresponding to n_{max} = 1.1, 2.4, and 4.8. These are associated with hard sphere, valence, and "doorway state" capture.

Fig. 7 *Classification of the different reaction types for low mass nuclides with A < 70 taken from Refs. [22,25] upper and lower plots, respectively. Note the similar values of the Eγ reduction exponent for direct and valence capture, The symbols k_{max} and m_{max} are the exponent values with the maximal correlation value, in our notation called L(max).*

The selection of data for these plots needs some explanation. The pronounced singularity, as shown in Fig. 4, requires two important conditions to be fulfilled:

1. The complete decay of the gamma - strength is required, the sum of partial primary absolute I_γ values should be close to $\Sigma I_\gamma = 100$.
2. The division of the total strength over large number of transitions and in a broad energy range (between $0 < E_\gamma < Bn$) are the most necessary features, often favoring the even-A product nuclei.

The accuracy of the L(max) determination depends primarily on the second condition and it has been estimated in Ref. [21] as close to 20%.

The following rules about $\rho = \rho(L)$ properties have been deduced in Ref. [21:

1. The nuclei with low correlation ($\rho < 0.5$) never show a singularity
2. Nuclei with strong correlation ($\rho > 0.5$) can be divided in three cases,
   a/ a clear singularity $0 < L(max) < 5$,
   b/ a suppressed singularity $L(max) = 0$, but ρ is maximal for $L < 0$ close to zero and
   c/ ρ is almost insensitive to L variation and this happens as L -> 5.

The cases b/ and c/ can be explained by abnormally wide or narrow energy regions.

The different capture reaction mechanisms with their characteristic behavior have been categorized and are displayed in the Table 2 taken from Ref. [25].

Table 2 Hierarchy of Reaction Mechanisms

Reaction Type	n Power of γ ray Energy	Correlations with
Direct Capture	1.2	S_{dp}
Valence Capture	2.3	S_{dp}, γ_n^2
Doorway (E1)	$\approx$ 5.0	S_{dp} or γ_n^2
Doorway (M1) $^{s}1/2 \rightarrow {}^{s}1/2$	$\approx$ 7 E_γ = 8 to 11 MeV	S_{dp}
Giant Dipole Resonance	$\approx$ 5.0	None

The quantities in the correlation column are the (d,p) spectroscopic factor $S_{dp} = (2J_f+1)S_n$ and γ_n^2 is the reduced neutron width of the initial state.

2.5 Recent analysis of the thermal capture for A < 70 using PSF data

It is a challenging task to review and to extend earlier results shown in Fig. 7 using the new information on the non-statistical models and further to explore the recent experimental data of E1 and M1 strengths behavior derived from the PSF studies.

Firstly, we have reviewed the (nγ)(dp) correlation using the earlier data base of the linear correlation coefficients ρ as a function of the exponent L of the E_γ^L reduction factor, varying L from 0 to 8, in Ref. [22]. Values of the correlation and its maximum L(max) are listed in Table 2. This exercise is described in detail and discussed in Refs. [19-21]. A similar limited analysis was carried out in Ref. [25] and the results are included for a comparison.

Table 2 Results of the (nγ)(dp) correlation analysis extracted from Refs. [22, 25] of the linear correlation coefficients of E_γ^L and $(2J + 1)S_n$ using data sources published before 1980. The quoted L(max) value corresponds to the correlation maximum. The (yellow, green and blue shaded) L(max) values represent respectively, the direct (hard sphere), resonant (valence) and statistical mode assigned in Ref. [25]. L(max) in the present notation equals to the n(max) used in Ref. [25]. For the grey shaded nuclides see Table 1 (no PSF data).

0* - the suppressed singularity (see Sect. 2.3)

0** - ρ is almost insensitive to L with negative or close to zero values

Target	$\sigma(\gamma)_0$	σ(B)	σ(D)	ρ (max)	L(max)	L(max)	n-max
	[b]	[b]	[b]	[22]	[22]		[25]
					ρ > 0.5	ρ < 0.5	
Na-23	0.525	0.012	0.057	0.51	0.59		
Al-27	0.231	0.130	0.108	0.86	1.8		1.2
Si-28	0.177	0.1285	0.132	1.00	0.95		0.91
Si-29	0.119	0.1173	0.078	0.94	1.4		1.25
P-31	0.166	0.1615	0.110	0.92	0.7		0.82
S-32	0.518	0.434	0.401	0.99	1.25		1.3
S-34	0.256	0.2535	0.224	0.97	0*		
Cl-35	43.6	43.6		0.09		0.09	
Cl-37	0.433	0.400	0.400	0.97	0.97		
Ar-36	5.2	5.2	**9.54**				1.2
Ar-38	0.8		0.46	0.97			
Ar-40	0.66	0.632	0.514	0.99			
Ar-41							1.15
K-39	2.1	2.08	0.753	0.39		0**	
K-41	1.46	1.355	1.32				
Ca-40	0.41	0.391	0.230	0.93	1.3		
Ca-42	0.680	0.639	0.680	0.99	1.15		
Ca-43	6.2	1.61		0.73	5		
Ca-44	0.88		0.865	0.99	1.15		
Ca-48	1.09	1.09	1.09		1.55		
Sc-45	27.2	26.33	**8.18**	0.02		5	
Ti-46	0.59	0.49	0.292	0.85	1.55		
Ti-47	1.63	0.74	**2.7**	0.39		2.3	
Ti-48	8.32	4.22		0.91	2.1		2.25
Ti-49	1.87	1.44	**2.01**	0.86	0.8		0.8
Ti-50	0.179	0.173	0.166	-0.27			
V-50	45	32.3					
V-51	4.94	1.32		0.30		0.8	
Cr-50	14.7	5.36	**9.6**	0.92	2.35		3.0
Cr-52	0.86	0.79	0.31	0.96	2.1		2.65
Cr-53	18.6	9.15	**17.8**	0.36		5	
Cr-54	0.41	0.375	0.278	0.97	1.5		
Mn-55	13.36	3.32		0.62	0*		
Fe-54	2.30	0.81	0.98	0.94	2.45		2.4
Fe-56	2.59	2.50	0.40	0.39			
Fe-57	2.48	1.34	**1.61**	0.70	0*		
Fe-58	1.32	1.11	**1.74**	-0.22		0**	
Co-59	37.18	7.62		0.35		0**	
Ni-58	4.39	4.07	**4.11**	0.93	0*		
Ni-60	2.45	1.01	1.09	0.98			5.0
Ni-62	14.9		**9.05**	0.41		5	5.0
Ni-64	1.63	0.91	1.37	0.80	4		4.05
Cu-63	4.50	4.097		0.11		5	
Cu-65	2.17	2.020		0.46		0**	
Zn-64	0.731	0.172	0.155	0.87	0*		

Zn-66	0.62	0.393	0.050	0.71	5		5.0
Zn-67	7.5	3.85		-0.38		5	
Zn-68	1.07	0.10	0.006				
Zn-70	0.092		0.039				

There are two ways to present the signatures of the non-statistical effects, either as a function of A or of the total thermal cross section. The latter approach has the advantage of an automatic preselection between non-resonant and resonant mode which is influenced by the size of the thermal cross section. The correlation results from the Table 3 are shown in Figs. 8 and 9. Fig. 8 shows the correlation coefficient ρ as a function of the total thermal cross-section. The dominance of the direct capture with a large correlation for σ(th) < 1 b is evident. For cross section above 1 MeV the trend of the correlation ρ begins to decrease, the distant levels contribution (resonant and non-resonant) starts to play its role and influence the value of ρ. For large cross sections, σ(th) > 10 MeV, the statistical capture takes over and the correlation disappears.

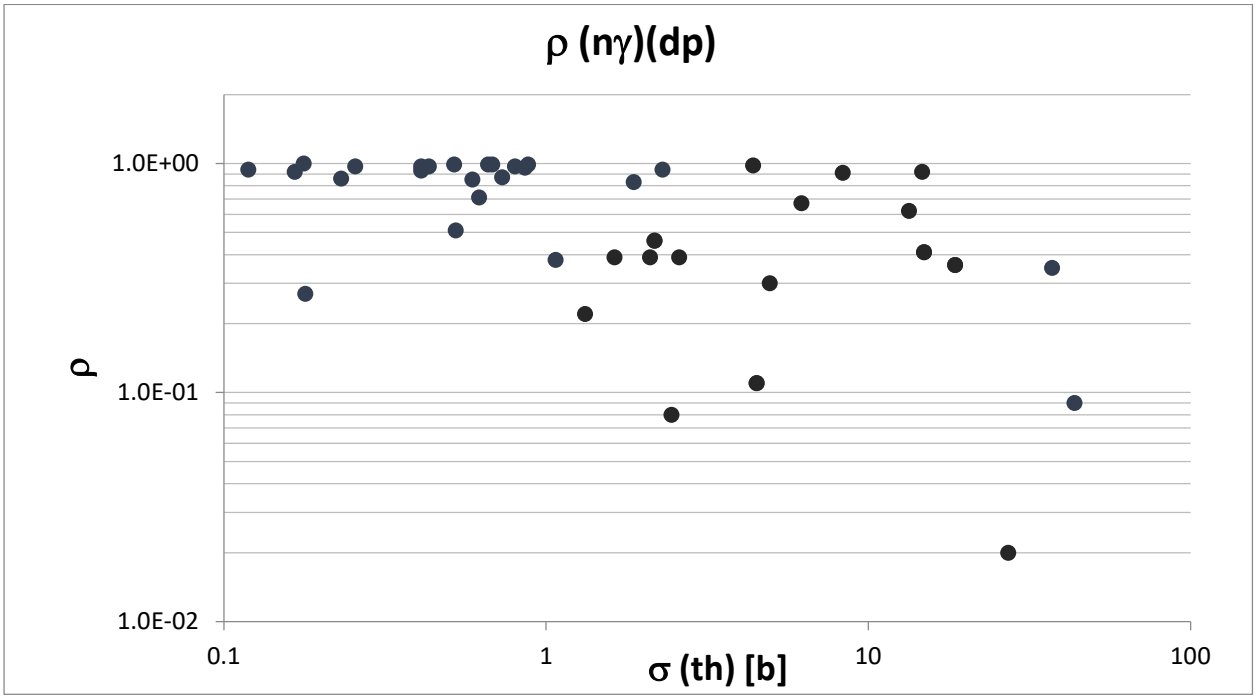

Fig. 8 *The plot shows the correlation coefficient ρ(max) of the (nγ) reduced intensities $I\gamma E\gamma^L$ and the spectroscopic $(2J_f+1)S_{dp}$ factors calculated in Ref. [22] for targets with A between 20 and 70. Note the decrease of the correlation with the increasing cross-section. The last three data points belong to cross-sections dominated by the compound nucleus model.*

Another quantity sensitive to the reaction process is the E_γ reduction exponent L, at which the correlation effect is maximal. The L(max) values are given in Table 3 in two columns marked as L(max). The criteria and their accuracy are discussed in Refs. [16-22]. In Fig. 9 is L(max) plotted as a function of the mass A and the data reveal two cross section groups, with σ < 1.5 b and σ > 1.5 b. The dominance of the potential hard sphere capture with L = 1 for targets with A < 50 is demonstrated in agreement with Figs. 7 and 8.

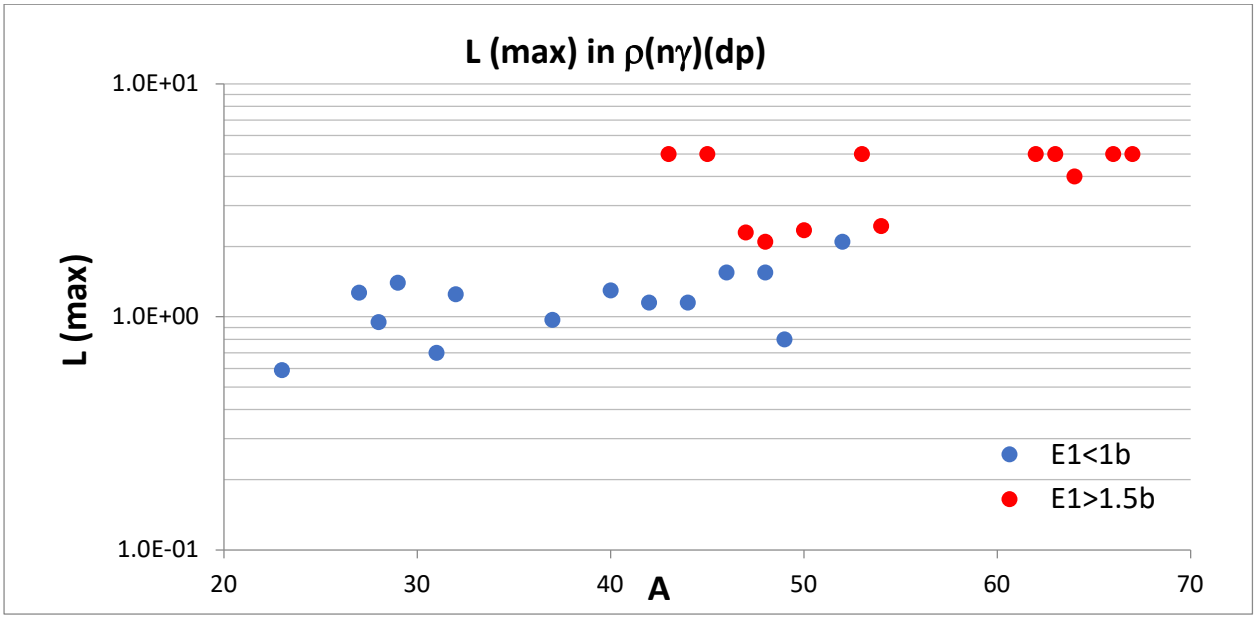

Fig. 9 *The E_γ^L reduction L value for the maximal correlation is plotted as function of the mass A. The data are divided in two groups for the σ(th) cross section limits < 1.5b (potential hard sphere capture) and > 1.5b (valence capture, with distant levels or resonance contributions).Note the clear dominance of L ~ 1 for A < 45 and a smooth increase to L ~ 5 up to A = 70.*

2.6 The PSF "slope" analysis

A new way to address the Eγ reduction exponent factor L, and the reaction mode, is to use the THC PSF data and to estimate the Eγ dependence of the data slope from the unweighted trend curves. This is demonstrated for the PSF data from the ^{45}Sc(n,γ) reaction, shown in Fig. 10, with trend lines in the E_γ^3 power format. The fitted equations are displayed in the figure as obtained from the Excel processing. At this point we need to bear in mind, that the PSF is defined in the Eγ-dipole space factor E_γ^3 format and the trend reduction exponent L can be calculated from the following relationship

$$L(\text{trend}) = L(\text{theory}) - 3 \qquad (4).$$

For example, the compound nucleus predicts L(trend) = 5 – 3 = 2. This is nicely confirmed in Fig. 10, the PSF DRC systematics (dotted green line) gives nicely the data slope L equals to 2.0.

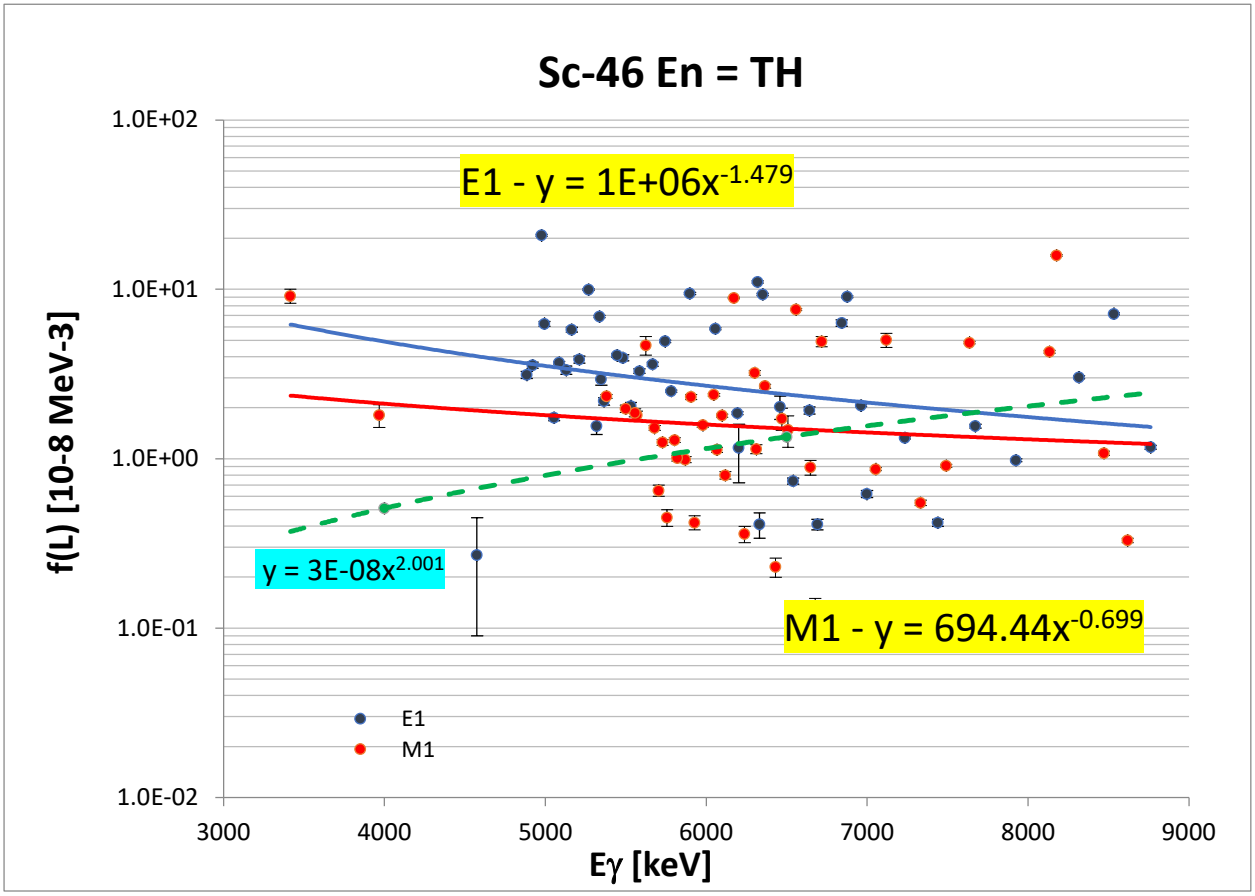

Fig. 10 *The E_γ dependence of reduced I_γ extracted from the PSF data of $^{45}Sc(n,\gamma)^{46}Sc$ reaction. The green dotted line represents the PSF E1 systematics from Ref. [2].*

The accuracy of the E_γ-dependence of I_γ/E_γ^L is strongly related to the number of data points and mainly to the sample size, given by the broadness of the energy region of the data. The unweighted trend derivation can be strongly influenced by a narrow energy region or by one or two extremely deviating data points. However, if enough nuclides are involved, a general conclusion can certainly be achieved. The L values of the reduced intensities I_γ/E_γ^L extracted from the PSF data are listed in Table 3.

Table 3 The list of relevant quantities needed for the qualification for the presence of the nonstatistical processes. All THC E1 data processed in the PSF format in Ref. [1] are quoted and extended by the recent PSF for ^{58,60}Ni and ^{64,67}Zn targets. If no entry for L and $\langle E\gamma^L \rangle$ is given, the entry was disregarded, either too small numbers of PSF data points or too narrow (< 1 MeV) energy region and or no data available.

Ra_s - the $|(R- a_s)/R)|$ factor indicating the presence of the distant levels (resonant) contribution (see Eq. (2)

L - the average E_γ exponent derived from the trend fit of PSF data

$\langle E\gamma^L \rangle$ - n(max) the real E_γ^n dependence of the gamma-ray strength decay

ρ - the linear correlation (nγ)(nd) coefficient (quoted if available in Refs. [22,25])

Target	$\sigma(\gamma)_o$	σ(res)/ $\sigma(\gamma)_o$	σ(B)/ $\sigma(\gamma)_o$	σ(D)	Ra_s|	$E\gamma^{min}$–$E\gamma^{max}$	<L>	<$E\gamma^L$>	ρ	ρ
	[b]			[b]		<MeV>	PSF slope	<Lmax>	nmax [22]	nmax [25]
F-19	0.0095	0.31	0.69	0.0047	0.03	0.6 – 5.6	-4.17	-1.17		
Na-23	0.525	0.98	0.02	0.057	0.28	1.6 – 3.6	-0.82	2.18	0.59	
Mg-24	0.0538	0.09	0.96	0.013	0.05	0.9 – 3.9	-0.39	2.61		
Mg-25	0.199	1	0		0.28					
Mg-26	0.0374	0	1	0.037	0.05					
Al-27	0.231	0.44	0.56	0.108	0.31	1.9 – 4.3	-1.67	1.33	1.8	1.2
Si-28	0.177	0.27	0.73	0.132	0.14				0.95	0.91
Si-29	0.119	0.01	0.99	0.078	0.08				1.4	1.25
Si-30	0.107	0.03	0.97	0.081	0.09					
P-31	0.166	0.01	0.97	0.110	0.17	1.7 – 4.7	-0.91	2.09	0.7	0.82
S-32	0.518	0.16	0.84	0.401	0.13	2.1 – 5.4	-0.64	2.36	1.25	1.3
S-33	0.454	0.009	0.99	0.157	0.23					
S-34	0.256	0.01	0.99	0.224	0.01					
Cl-35	43.6	0.002	1		2.0	1.9 – 6.6	-1.60	1.40	0.09	
Cl-37	0.433	0.21	0.92	0.400	0.11	1.3 – 6.1	-1.01	1.99	0.97	1.1
Ar-36	5.2	0	1	**9.54**	7.77					1.2
Ar-38	0.8	0	0	0.46	0.44					
Ar-40	0.66	0.04	0.96	0.514	0.25					
K-39	2.1	0.01	0.99	0.753	0.52	2.3 – 7.8	-0.76	2.24		
K-41	1.46	0.24	0.76	1.32	0.02					
Ca-40	0.41	0.05	0.95	0.230	0.42	3.6 – 6.4	-0.60	2.40	1.3	
Ca-42	0.680	0.06	0.94	0.680	0.07				1.15	
Ca-43	6.2	0.74	0.26		0.57				5	
Ca-44	0.88	0.06	0	0.865	0.59				1.15	
Ca-48	1.09	0	1	1.09	0.84				1.55	
Sc-45	27.2	0.03	0.97	**8.18**	2.72	4.6 – 8.8	-1.48	1.52	5	
Ti-46	0.59	0.06	0.83	0.292	0.26					
Ti-47	1.63	0.55	0.45	**2.7**	0.03				2.3	
Ti-48	8.32	0.49	0.51		0.51	2.3 – 6.8	1.79	4.79	2.1	2.25
Ti-49	1.87	0.23	0.77	**2.01**	0.77				0.8	0.8
Ti-50	0.179	0.03	0.97	0.166	0.31					
V-50	45	0.28	0.72		0.33	4.1 – 9.4	0.10	3.1		
V-51	4.94	0.73	0.27		0.92	3.5 – 7.3	2.45	5.45	0.8	
Cr-50	14.7	0.64	0.38	**9.6**	0.1	5.2 – 8.5	2.67	5.67	2.35	3
Cr-52	0.86	0.08	0.93	0.31	0.05				2.1	2.65
Cr-53	18.6	0.50	0.50	**17.8**	0.26				5	
Cr-54	0.41	0.09	0.91	0.278	0.17				1.5	
Mn-55	13.36	0.75	0.25		0.18					
Fe-54	2.30	0.65	0.35	0.98	0.29				2.45	2.4
Fe-56	2.59	0.03	0.97	0.40	0.71	2.4 – 7.6	1.56	4.56		
Fe-57	2.48	0.46	0.55	**1.61**	0.63	4.6 – 10.0	-2.51	0.49		
Fe-58	1.32	0.16	0.84	**1.74**	0.88					
Co-59	37.18	0.80	0.21		0.63	3.9 – 7.5	0.84	3.84		
Ni-58	4.39	0.07	0.93	**4.11**	1.25	3.9 – 9.0	1.50	4.50		

Ni-59	73.7	1.0								
Ni-60	2.45	0.59	0.41	1.09	0.58	3.4 – 7.8	4.14	7.14		5.0
Ni-61	2.1	0.25	0.75		0.17					
Ni-62	14.9	1	0	**9.05**	0.29	2.4 – 6.8	1.34	4.34	5	5.0
Ni-64	1.63	0.44	0.56	1.37	1.05				4	4.05
Cu-63	4.50	0.10	0.91		0.04	3.6 – 7.9	-0.21	2.79	5	
Cu-65	2.17	0.07	0.93		0.58	3.6 – 7.1	-1.83	1.17		
Zn-64	0.731	0.77	0.23	0.155	0.20	4.8 – 7.9	1.81	3.1		
Zn-66	0.62	0.37	0.63	0.050	0.04					5.0
Zn-67	7.5	0.49	0.51		0.22				5	
Zn-68	1.07	0.91	0.90	0.006	0.03					
Zn-70	0.092	1	0	0.039	0.13					

The results of the L(max) determination from PSF processing are shown in Fig. 11. This figure can be compared with Fig. 7, originating from Ref. [25], and they are rather similar. The scatter of derived nmax points in Fig. 7 is smaller, this can be explained that the use of the (nγ)(dp) correlation is more accurate then the slope trend tool from the PSF data. Similar conclusions can be made concerning the classification of the non-statistical processes. The region below $A \simeq 50$ is fully dominated by the direct capture of the elastic potential scettering. Going up to heavier targets, a smooth transfer to resonant (distant level) contribution takes place, however, both processes can be present together and this fact may influence the PDF data slope as well as the 'n_{max}' value.

The overlap of these two approaches demonstrates in Fig. 12 nicely demonstrates a very similar trend and distribution of the L(max) values derived with two different methods of the same thermal capture data. The only difference is, as pointed out earlier, a slightly increased n_{max} for the pure hard sphere direct capture, which probably comes from the very simplified slope determination from the PSF data.

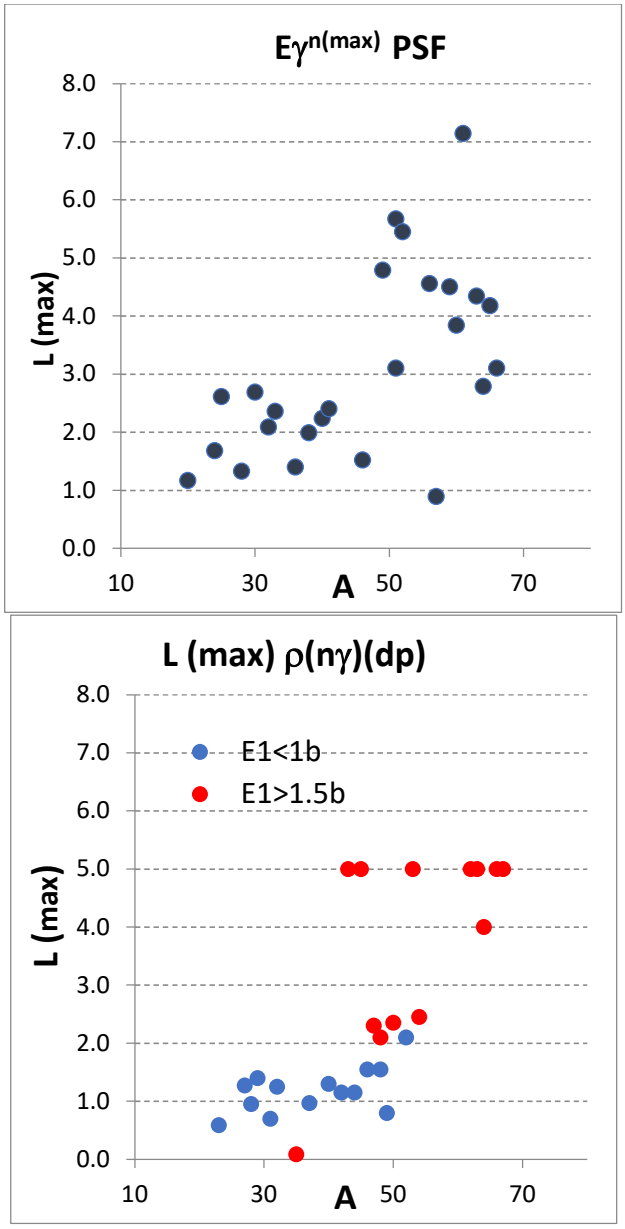

Fig. 11 *Values of L(max) derived from the "slope" analysis of the PSF data. Note a similar trend for A < 50 and A > 50 data as in Fig. 7. Two outliers (^{57}Fe and ^{61}Ni shown as larger points) are discussed below.*

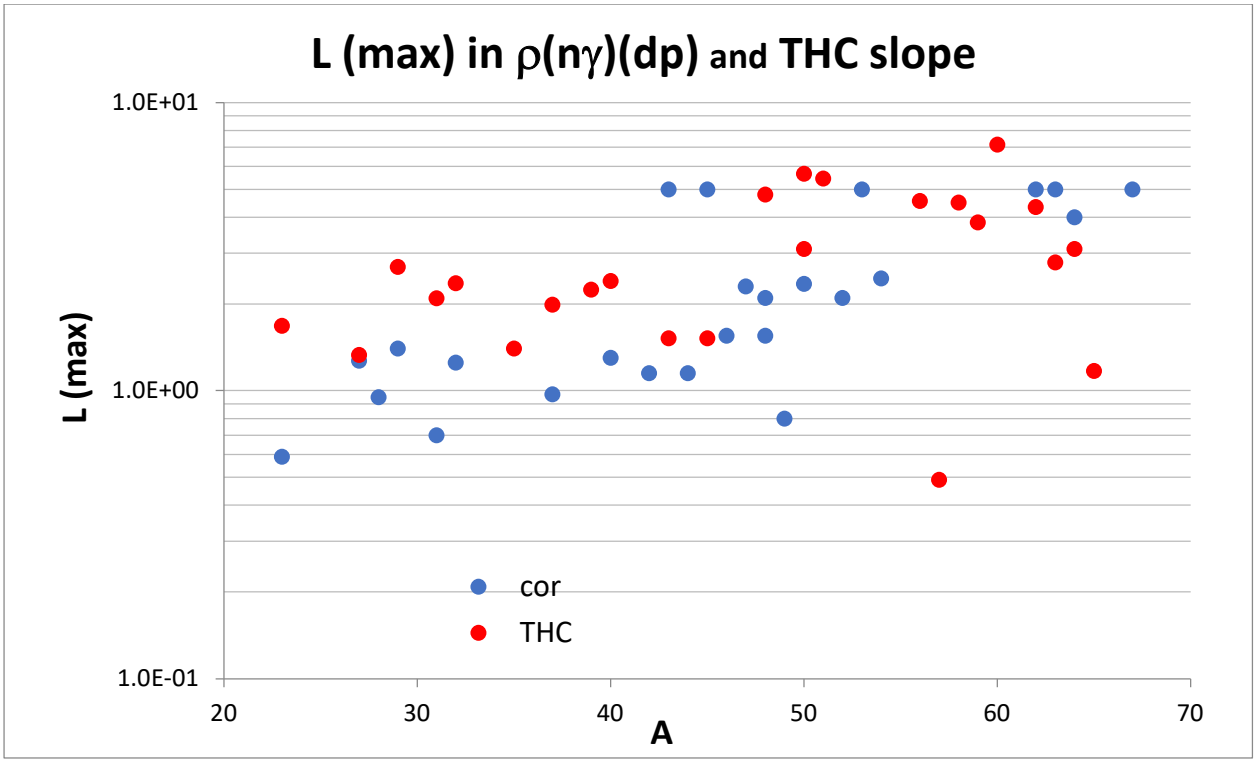

Fig.12 *Data (cor) from the correlation (nγ)(dp) analysis plotted together with the results determined from the slope analysis of the PSF thermal capture data (THC).*

An interesting outlier is the ^{57}Fe(n,γ)^{58}Fe reaction. The thermal cross section of 2.48 b is formed by three s-resonances with Ji = 0^- (25%) and 1^- (75%), respectively. The bound levels contribution of 1.34 b is fitted by two states with -0.22 and -55 keV energies and spin $J_i = 1^-$. We can therefore conclude that the dominating spin of the capture state is $J_i = 1^-$. The PSF results are shown in Fig. 13 and the primary gamma ray strength is exclusively (93%) the E1 mode with no M1 transition detected (lack of adequate negative parity states?). The data sample used for the slope identification is sufficiently wide and the number of data points is large.

The direct capture calculated cross section (see Table 3) amounts to 1.61 b, which can explain the complete σ(B) and the value of $|(R- a_s)/R)| = 0.63$ allows some distant levels contribution. The possible explanation, quite speculative, may be that the hard sphere direct capture prefers the feeding of states ($p_{1/2}$ and $p_{3/2}$) below 7 MeV differently. The answer is not clarified by the (nγ)(dp) correlation with r = 0.7 with the suppressed L(max) = 0.

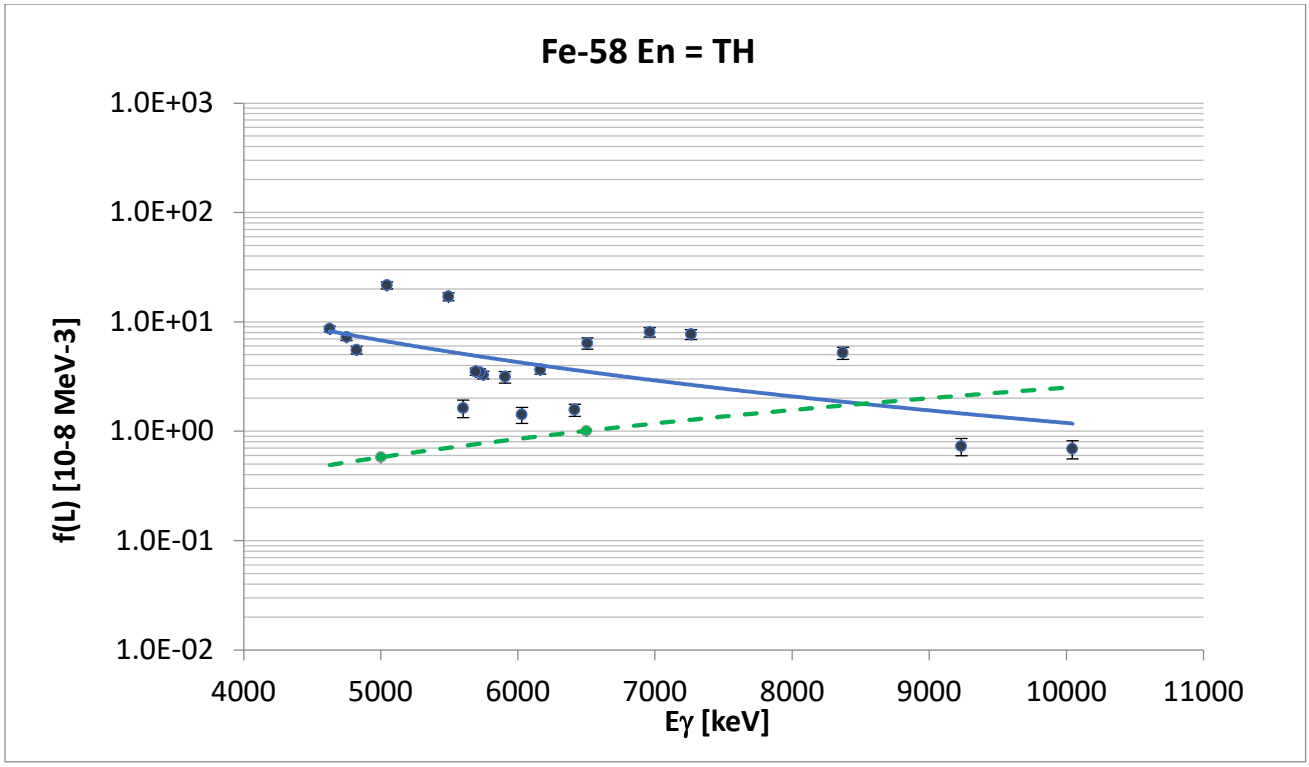

Fig. 13 *The E1 PSF data of ^{58}Fe nuclide to final states with solid positive parity assignments. The PSF systematic E1 prediction is shown as the green dotted curve.*

The ^{61}Ni outlier is an example of the influence of several points quite far from the expected data dispersion, note the first two points in Fig. 14. The trend, however, is in a reasonable agreement with the PSF systematic prediction (green dotted curve) and the larger value of L(max) = 7.14 can be associated with the expected value of 5. We may conclude that this case is not a principal outlier but influenced by the first two extreme data points. This feature shows how is the trend slope method dependent on the "quality" of the data points sample.

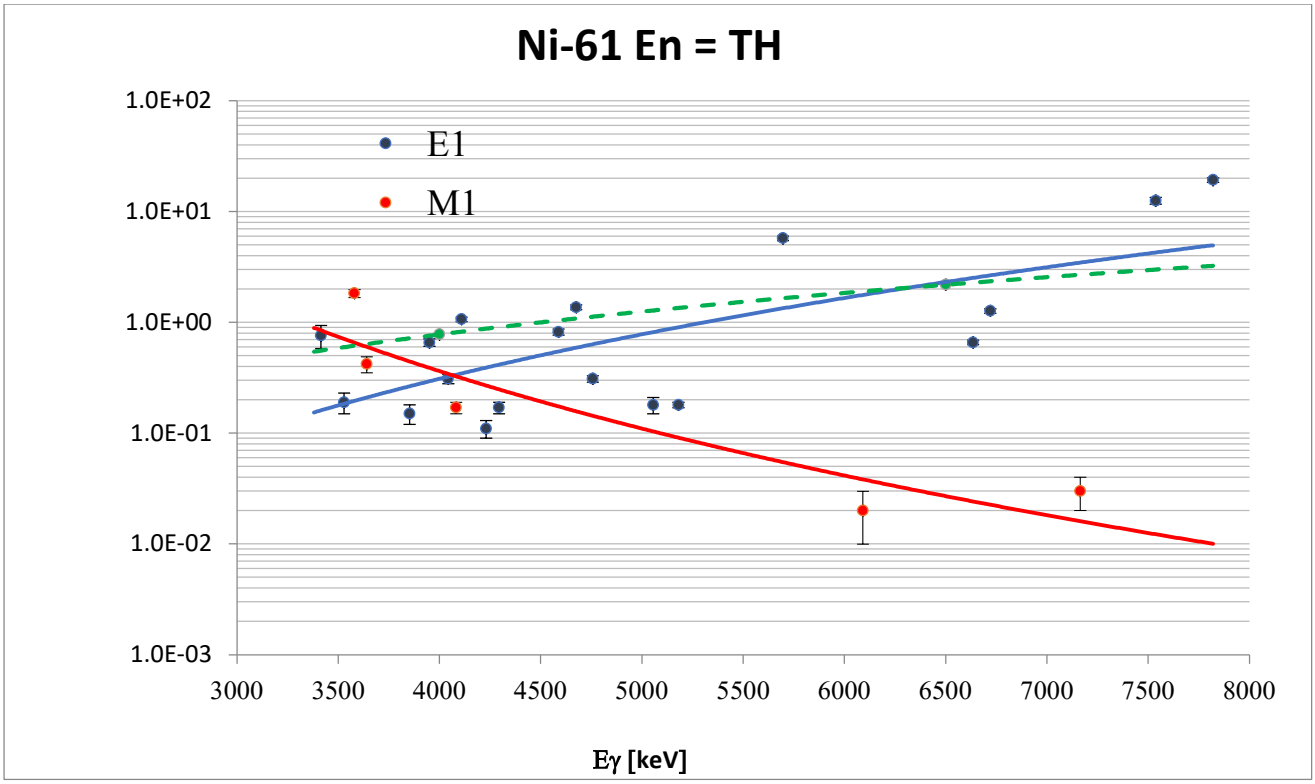

Fig. 14 *The ^{61}Ni PSF thermal data for E1 and M1 transitions. The green dotted line is the PSF systematic E1 prediction. Note the agreement of E1 and systematic curves.*

2.7 Properties of the thermal capture for A < 150 (3s -> 2p region)

The (4s – 3p) giant resonance forms another mass region around A ~ 150 in which the direct capture was predicted as shown in Fig. 3. Especially nuclides at the beginning this region, between 130 < A < 160, have calculated values of s(D) between 0. 1 and 1. 5 b [15]. The ATLAS_f(L)_THC database includes nine nuclides between 90 < A < 154 and therefore we have decided to analyze these data in a similar way as the light nuclides in the previous sections. The positive non-statistical effect was observed in the ^{136}Xe(n,γ)^{137}Xe reaction and published in Ref. [26]. The correlation analysis is shown in Fig. 15 taken over from [26]. The calculated partial DRC E1 intensities were in a very good agreement with the experimental values. This is the only publication dealing with the non-statistical effects in the (3s – 2p) region we found.

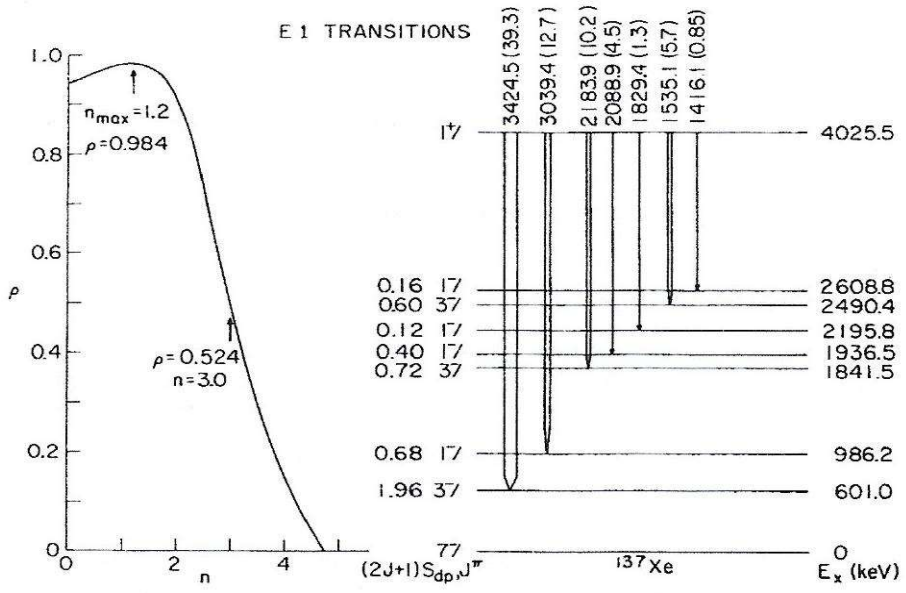

Fig. 15 *The variation of the correlation coefficient with the reduction E_γ factor for the $^{136}Xe(n,\gamma)^{137}Xe$ reaction. The right-hand side of the figure shows the primary E1 transitions involved. Note that ρ is maximal at n ~ 1.2, the signature of the direct hard sphere capture.*

The $^{136}Xe(n,\gamma)^{137}Xe$ reaction has a very specific reaction parameters, very low neutron binding energy B_n = 4026 keV with rather small thermal cross section σ(th) = 0.26 b. There is negligible resonant contribution to this cross section and fully allocated to σ(B) and the calculated direct capture amounts to σ(D) = 0.192 b. The $p_{1/2}$ and $p_{3/2}$ final states are available at very low energies what results in primary transitions of a very small energies (note the decay scheme in Fig. 13). We have carried out the standard PSF analysis and the result is shown in Fig. 16.

The applied slope analysis resulted in <L> = 0.04 which gives <Lmax> for the <$E\gamma^L$> reduction equal to 3.04 and disagrees n_{max} = 1.2 from Fig. 13. This case clearly demonstrates the sensitivity of the unweighted trend procedure to the "quality" of the data sample. However, we need to distinguish between increasing and decreasing trend of the E1 strength with the decreasing energy E_γ. The postulated power dependence is not physically grounded but as a mean representation defendable, but in Fig. 16 the right-hand plot shows the polynomial fit which looks even better.

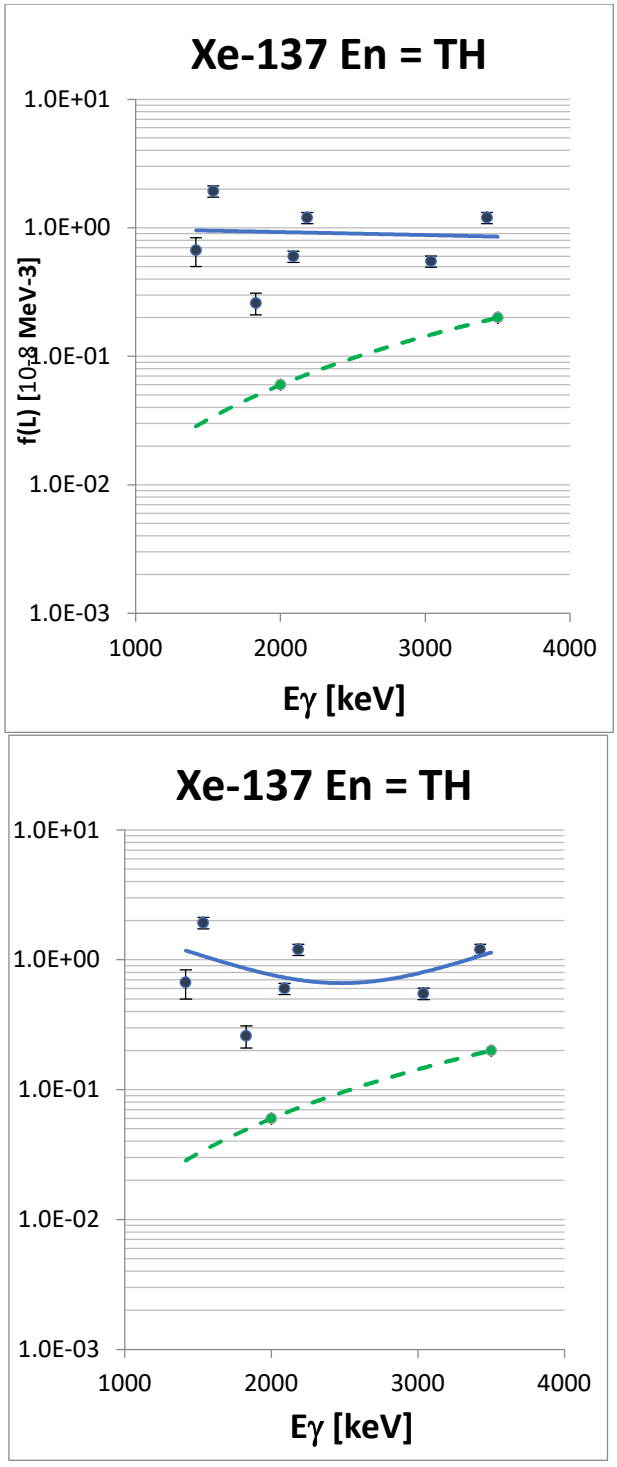

Fig. 16 *The ^{137}Xe PSF thermal data for E1 transitions. The green dotted line is the PSF systematic E1 prediction, note the huge overestimation of the thermal data. The power and polynomial dependence fits are used in the left – and right-hand plots, respectively.*

The nuclides with A > 90 from the TH PSF data base are listed in Table 4 together with their cross- section behavior and the results of the slope analysis. All selected nuclei have very large

thermal cross-section and except one (^{137}Ba) no direct capture has been predicted. The compound nucleus mechanism via resonant contributions, both from positive and negative resonances, is expected to be dominant.

Table 4. The list of heavier nuclides processed in the ATLAS_f(L)_THC PSF data base. Note that only for one target (^{137}Ba) was the σ(D) calculated. Data disregarded if $\Delta E_\gamma < 1$ MeV.

Target	$\sigma(\gamma)_0$	$\sigma(res)/\sigma(\gamma)_0$	$\sigma(B)/\sigma(\gamma)_0$	σ(D)	$E\gamma^{min}$–$E\gamma^{max}$	<L> PSF slope	$<E\gamma^L>$
	[b]			[b]	[MeV]		
Nb-93	1.15	0.08	0.92		5.7-6.8	6.25	9.25
Rh-103	143.5	0.94	0.06		5.7-7.0	-4.0	-1.0
Pd-105	21.0	0.11	0.89		6.6-7.2		
F I-127	6.15	0.64	0.36		5.1-6.7	1.60	4.60
Cs-133	30.0	0.68	0.32		5.6-6.7	-5.09	-2.09
Ba-135	5.8	0.39	0.61		6.1-6.7		
Ba-137	3.6	0.01	0.99	0.20	4.8-5.7		
Nd-146	50	0.06	0.84		4.6-7-1	7.0	10.0
Eu-154	312	0.18	0.82		6.1-6.6		

The PSF analysis of the ^{137}Ba(n,γ) thermal capture is shown in Fig. 17 taken from Ref. [1]. The E1 strength reasonably agrees with the systematic prediction and the slope, due to few data points in a narrow E_γ range, is associated with a large uncertainty which masks any serious conclusion on the slope and L(max) values.

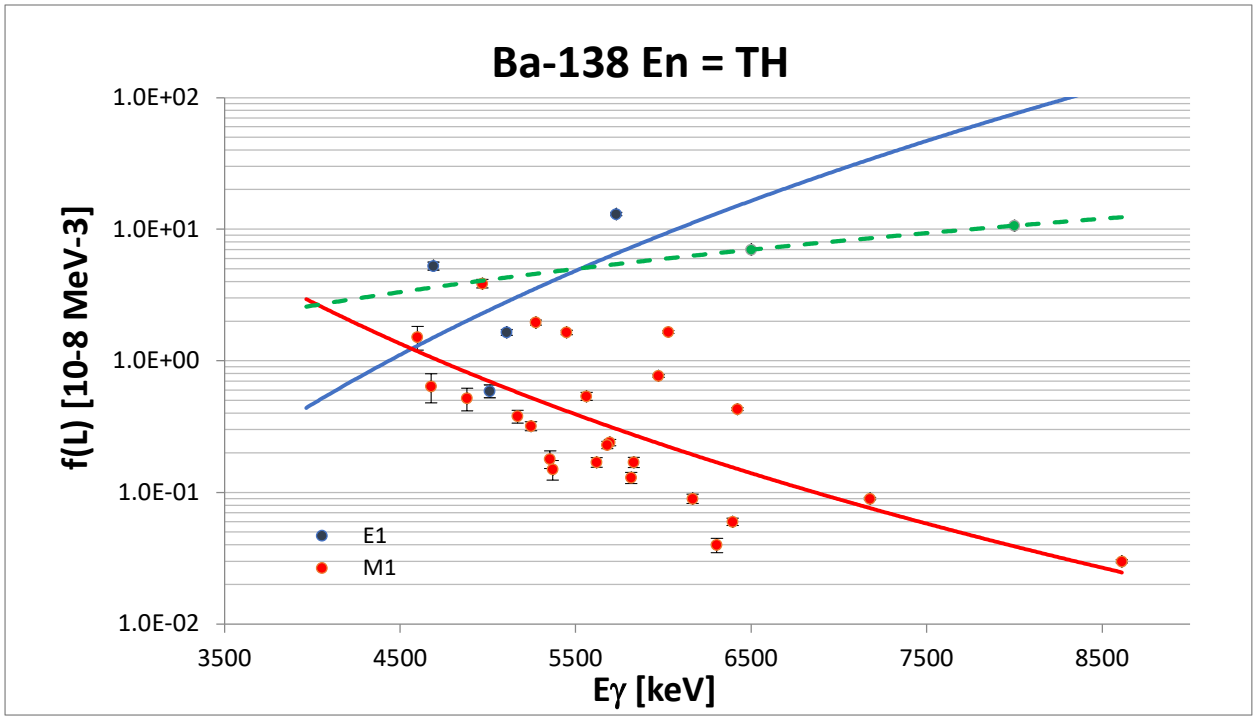

Fig. 17 *The ^{138}Ba PSF thermal data for E and M1 transitions. The green dotted line is the PSF systematic E1 prediction for E1 strength.*

The slope analysis have been carried out for all nuclides with A > 90, the results are shown in the two last columns of Table 4. The relatively narrow E_γ energy regions limited the accuracy of the analysis, the dispersion of data is too large as shown in Fig. 18. We provided therefore the mean value of all data which, is <L(max)> = 5.4, as the representative value for this mass region which is in a good agreement with the expected dominance of the compound nucleus model.

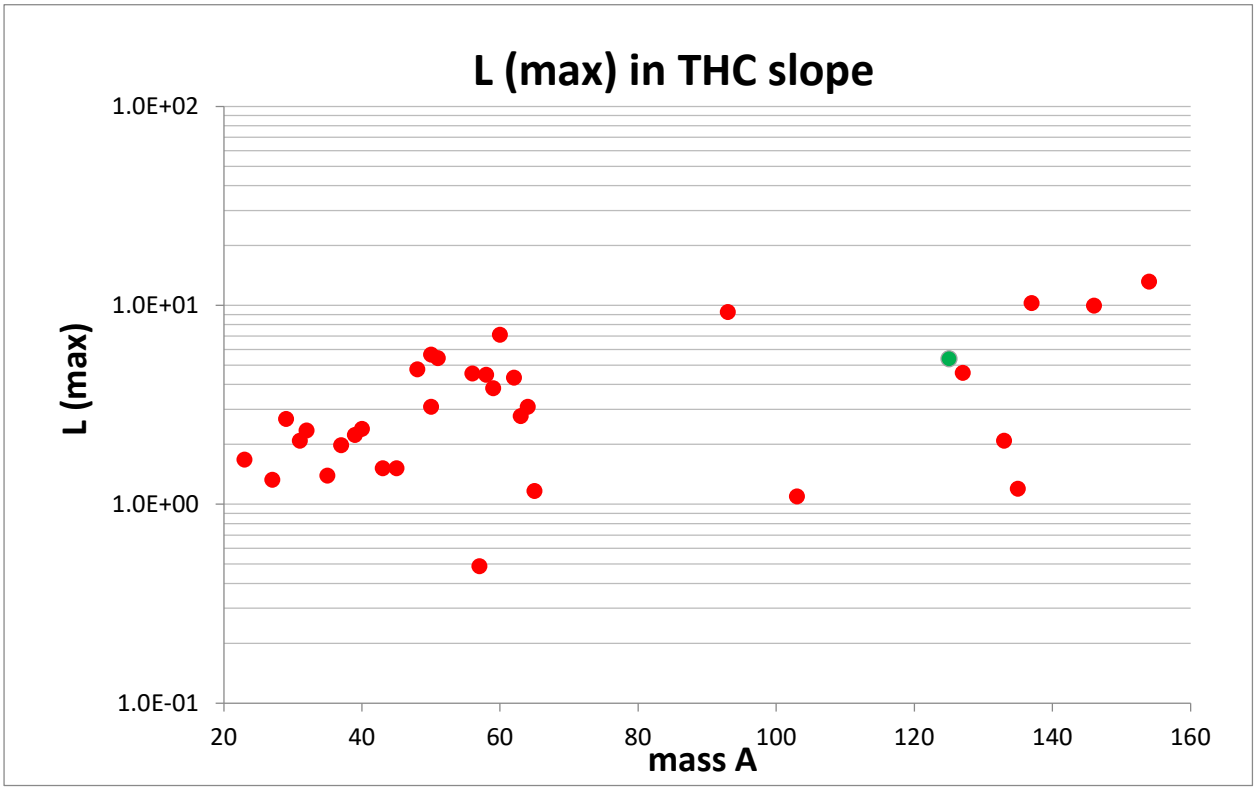

Fig. 18 *The L(max) derived from the slope analysis for all nuclei. Note the scatter of the data points for the data above A > 90 and the mean value (green point) <L(max)> = 5.4*

We may conclude that the slope method losses its power to detect the non-statistical effects for increasing mass and the decrease of the energy region width of the primary E1 transitions. In order to facilitate more details and evidence of the non-statistical effects in this mass region the PSF analysis of the low cross section targets is recommended.

2.8 Conclusions of E1 strength behavior in the A < 70 region

The E1 thermal capture behavior and the underlying reaction models for nuclides with A < 70 have been reviewed using the earlier results and extended with the recent PSF data [1]. The PSF data have been used in a novel manner to identify the reaction processes which govern the thermal capture in the (3s – 2p) giant resonance region, forecasted as the region dominated by non- statistical effects.
The recent conclusions and observations can be summarized as such:

1. E1 transitions are the major decay process accounting for about 94 % of the total strength in thermal capture. This conclusion is based on the study of partial thermal cross sections where the deficit of σ(th) from the positive resonance contributions σ(B) can be for many nuclides be explained as a non-resonant cross section in the frame of the Lane-Lynn theory of the direct capture. When considering targets with mass close to A = 50, the distant levels valence and resonant capture start to contribute.

2. This conclusion has been verified by two independent methods applied to the thermal capture spectra. Firstly, the correlation analysis of the reduced (n,γ) intensities I_γ and the (p,d) final state spectroscopic factors $(2J_\gamma +1)S_n$ fully supports the above statement and further the correlation dependence of the ρ(max) as a function L in the reduction factor E_γ^L form an effective signature of the non-statistical reaction mode.

3. The second analysis involved is the use of the PSF thermal data, in which the trend slope of the PSF as a function of E_γ forms another signature for the presence of the non-statistical effects. The agreement between these two approaches was the major achievement in this paper and is a very important argument for the verification of the processing applied to the PSF data.

4. The enhancement of E1 strength against the statistical predictions can be explained by dominance of the direct capture (DC) over the statistical model (CNM) in this mass region.

3. General remarks on M1 enhanced transitions

3 .1 Historical survey

The primary M1 strength was not consistently addressed during the inventive period of the Direct Capture Theory in the seventies, probably due to its relatively small contribution to the thermal cross section. Another reason may be that the direct M1 process is under the assumptions of the Single Particle Model (SPM) is forbidden for $s_{1/2}$ –> $s_{1/2}$ transitions. Bohr and Mottelson [27] proposed a giant resonance with a spin flip mechanism to account for the observed enhancement of M1 radiation over the Weisskopf SP prediction. The M1 transition strength distribution was expected to follow the statistical model. The spin-flip resonance energy E_o was predicted to depend on the mass A as $E_o = 41\ A^{-1/3}$ MeV. This equation brings the resonance energy above the neutron binding energy of light nuclides and its tail below B_n is important.

Fractions of the total thermal capture of E1 and M1 strengths for the studied nuclides are shown in Table 5. Note that comparable contributions of E1 and M1 strength are present only in very light nuclei for A> 46 become negligible. This is mainly due to the limited availability of suitable final states in that region.

Table. 5 The total absolute primary strength of E1 and M1 radiation and the energy range of measured M1 transitions. The range in italic has only one single M1 transition.

Product nucleus	**Σ I_γ (E1)**	**Σ I_γ (M1)**	**E1/M1**	**Σ (tot)**	**M1 E_γ range ΔE**
	(%) abs.	(%) abs.		(%) abs.	[MeV]
					low- high
F-20	59.6	40.1	1.5	99.7	0.3 – 6.6
Na-24	24.1	75.1	0.32	99.2	0.7 – 6.5
Mg-25	96.1	5.3	18.1	101.4	2.2 – 6.8
Mg-26	16.8	69.7	0.24	86.5	3.9 – 11.1
Mg-27	82.4	19.2	4.3	101.6	1.0 – 5.5
Al-28	48.0	53.1	0.90	101.1	0.5 – 7.7
Si-29	89.4	9.9	9.3	99.3	1.6 – 8.5
Si-30	75.3	24.6	3.1	99.9	4.0 – 10.6
P-32	63.1	35.3	1.8	98.4	1.2 – 8.0
S-33	92.3	6.9	13.4	99.2	2.0 – 8.6
Cl-36	48.5	44.6	1.1	93.1	2.0 – 8.6
Cl-38	91.0	0.7	130	91.7	*4.2*
K-40	78.7	13.7	5.7	92.4	4.0 – 5.5
Ca-41	81.1	4.8	16.9	85.9	3.4 – 6.4
Sc-46	42.4	36.8	1.2	79.2	3.4 – 8.6
Ti-49	98.2	0.8	122.3	99.0	2.7 – 5.6
V-51	66.1	3.4	19.4	69.5	4.0 – 4.1
V-52	92.0	3.5	26.3	95.5	1.6 – 5.6
Fe-57	93.5	5.2	18	98.7	2.4 – 5.3
Fe-58	100			100	-
Co-60	72.5	1.8	40.3	74.3	2.6 – 5.1
Ni-59	99.2	1.8	55.1	100.0	*5.3*
Ni-61	99.2	1.7	58.4	100.9	3.6 – 4.1
Ni-63	98.0	2.4	40.8	100.4	3.1 – 3.6
Cu-64	77.0	2.0	38.5	79	3.4 – 6.7
Cu-66	72.0	8.6	8.4	80.6	2.5 – 4.9
Zn-64	94.8	5.4	17.6	100.2	3.6 – 6.1
Zn-68	92.1	8.0	11.5	100.1	4.9 – 7.4
Mean value	<76>	<18>	<24>	<94>	

The division of E1 and M1 decay strength is demonstrated in Fig. 19. The dominancy of the E1 mode is clearly seen with the sharply D1Minishing M1 decay for heavier masses. The lack of M1 decay for targets with A > 45 is probably due to the absence of suitable final states in the corresponding energy range and from the position of the spin-flip resonance at higher energies. This latter observation is supported by the width ΔE of the M1 transitions window and its position relative to the "spin-flip" energy E_o (see the last column in Table 5 and Fig. 20).

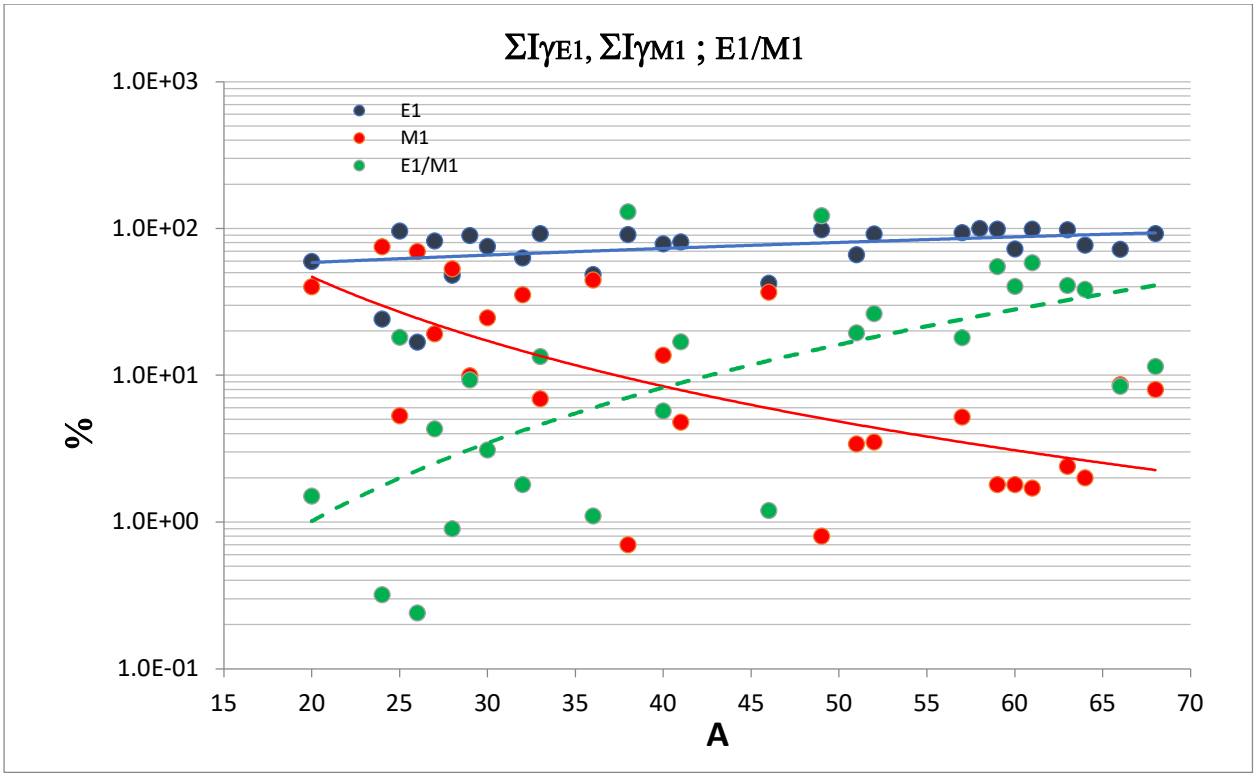

Fig. 19 *The total absolute primary strength of E1 and M1 radiation. The green dotted line reflects the dependence of the E1/M1 ratio on the mass. Note the large E1/M1 at A ~ 60 approaching a value of about 25. All curves represent the unweighted power trend lines.*

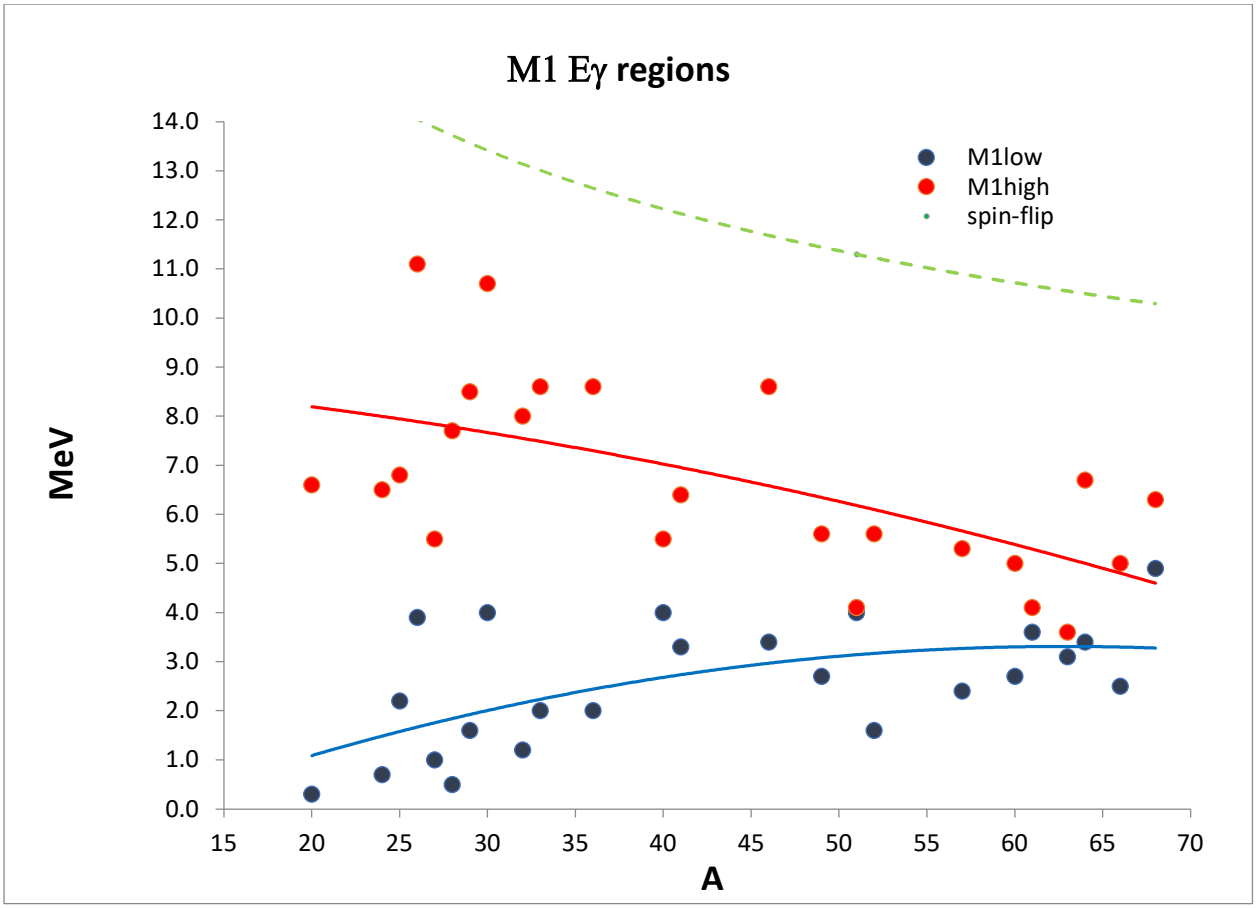

Fig. 20 *The red and blue curves represent the unweighted power trend lines of the low/high energies of the M1 transitions window. The spin-flip curve follows the systematic prediction of* $E_o = 41\ A^{-1/3}$ *[26]*

The stronger M1 strength for targets with A < 40 suggests the possibility of another process in addition to the statistical one. However, none of the non-statistical effects, so strongly present in the E1 capture, are expected for M1 transitions. For thermal capture they should be of $3s_{1/2}$ -> $2s_{1/2}$ or $1d_{3/2}$ character, both forbidden in the SP model. It was therefore quite surprising that Kopecky [28] observed a (nγ)(dp) positive correlation for M1 transitions to $l_n = 0$ but not to $l_n = 2$ orbitals. The results of this analysis are shown in Table 6. This surprising observation was supported by the non-statistical behavior of M1 transitions in the capture spectra from two neighboring s- and p-wave resonances in the ^{35}Cl target [29].

The theoretical explanation was proposed by Clement and Lane in Ref. [30] as a semi-direct capture mechanism. The incident s-wave neutron excites the giant M1 resonance which emits gamma-rays as it decays to s- or d- wave states. Mughabghab in Ref. [25] speculated that the energy and/or the width of the M1 resonance are expected to be smaller (see Ref [27]) than for GE1R and consequently the energy dependence can be even faster than $E\gamma^5$. The results of a limited test are shown in Fig. 21, where the bell shape dependence for ^{25}Mg and ^{35}Cl supported the faster E_γ dependence. The sharp decrease of the correlation curve for ^{27}Al above L > 4 is difficult to explain as well as the maximal correlation at L = 0. The energy width ΔE of the M1 window is quite broad and that excludes it as a contribution, although with less certainty. However, the limited number of targets makes his analysis not relevant for the whole mass region.

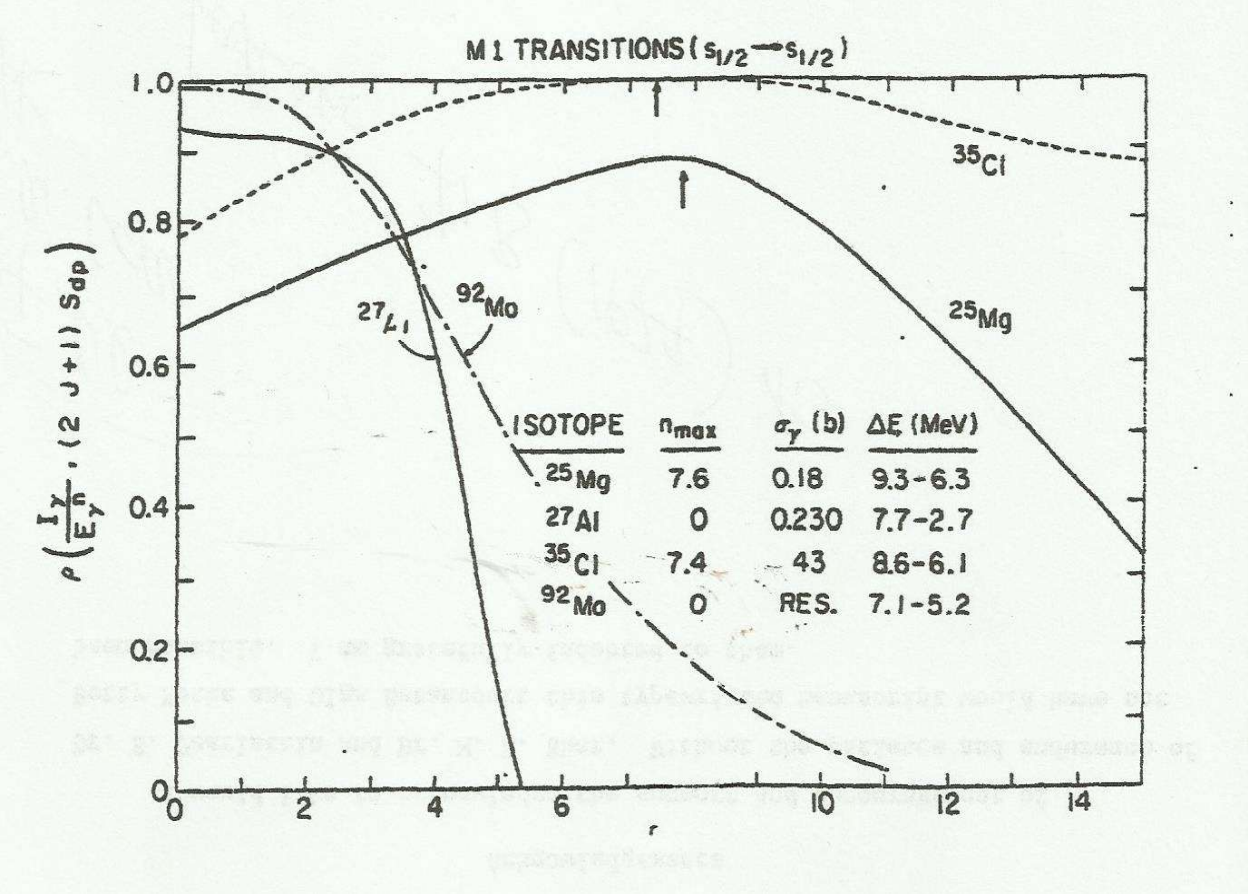

Fig. 21 *The (n,γ)(d,p) correlation analysis from Ref. [26]*

Kopecky later has extended this analysis up to A ~ 130 and presented the results at the Berkeley Conference in 1980 [31,32]. The Abstract of Ref. [32] is included here as a conclusion. To our knowledge this was the last comprehensive work of this kind on the M1 enhanced strength. All details and logbooks of this presentation were unfortunately lost in connection with the retirement of the author. The accuracy of the correlation degree can be estimated from the figure in the Abstract.

NONSTATISTICAL FEATURES OF M1 TRANSITIONS NEAR NEUTRON THRESHOLD

J. Kopecky

Netherlands Energy Research Foundation
1755 ZG Petten, The Netherlands

Recently the interest in M1-neutron capture has grown, because beside larger transition strength than predicted also (n,γ) (d,p) correlations have been observed. Since the direct s-s(d) capture is forbidden, Clement et al.[1] attributed the correlation to a semidirect process, in which two conditions have to be fulfilled for a large effect: the target nucleus has a collective M1-giant resonance with energy $h\omega_1$ and in the product nucleus bound states (l_n=0) are available at excitations E_x, such that $B_n - E_x \simeq h\omega_1$. These conditions eliminate closed-shell nuclei and mass ranges 40-80 or 130-220 (s-orbits are filled).

In order to provide more experimental information on correlations for s-s transitions, a systematic study has been made for A < 130 (see fig. 1) and the following conclusions can be drawn: (i) Significant correlation is concentrated in 5 odd targets with $25 \leq A \leq 35$, the only exception is ^{92}Mo (perhaps ^{102}Ru too). (ii) The abrupt cut-offs of the correlation at A=25, 35 can be well understood. For A < 25 the M1-matrix element falls to zero, as $A \rightarrow {}^{16}$O ($1d_{5/2}$ orbit is empty), while for A > 35 the $2s_{1/2}$-final orbit is fully occupied, i.e. not available and the M1-matrix element falls again to zero, as $A \rightarrow {}^{40}$Ca ($1d_{3/2}$ orbit is full). (iii) Large correlation found for ^{35}Cl and ^{92}Mo, where resonances are strongly involved, was however difficult to explain with the semidirect model only and valence components had to be considered too [1]. (iv) The correlation is almost absent in the mass range 80 < A < 130, which is surprising, because the facts are similar to those in $25 \leq A \leq 35$.

Very recently some evidence occurred, which may help us to understand the last two riddles. Lane[2] pointed out, that strong initial correlations can in fact arise from the semidirect process as well and this is just important to preserve the effect in nuclei, where resonances are involved.

Another vital information has been given in the dynamical theory of GDR[3], which predicts a spreading of the M1 strength to substantially higher excitations than previously foreseen for nuclei heavier than Ni isotopes. This may break the condition of the energy match for masses 80 < A < 130.

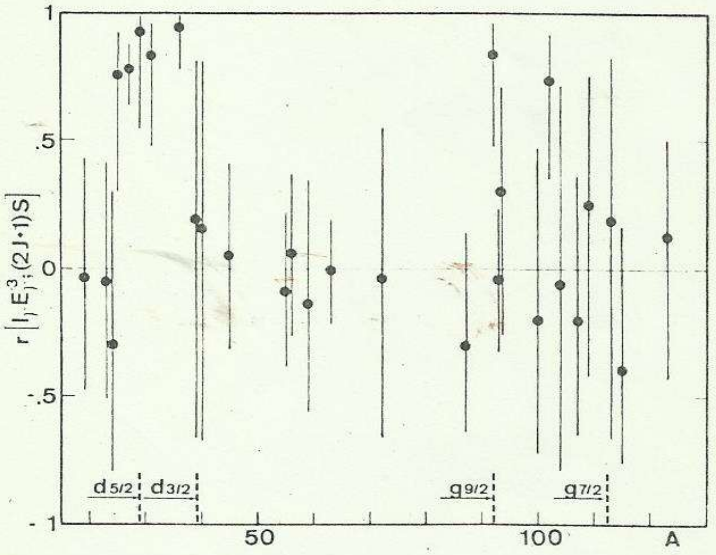

Fig. 1. Linear correlation coefficient r vs A. Error bars represent rms errors based on Fisher's transformation.

1. C.F. Clement, A.M. Lane, and J. Kopecky, Phys. Lett. 71B (1977) 10
2. A.M. Lane, Inv. paper at Conf. on "Statistical Properties of Nuclei", Hvar, Yugoslavia, October 1 (1979)
3. G.E. Brown, J.S. Dehesa, and J. Speth, Nucl. Phys. A330 (1979) 290

Table 6. The (nγ)(dp) correlation of M1 transitions for nuclides with A < 72. N_f is the number of analyzed final states and I_γ was reduced by the standard E_γ^3 factor. The data from Ref. [32] were extracted from the figure in the Abstract and are printed in italic. The last two columns show the results from Ref. [25] in which the reduction factor L was used as a variable to obtain the maximal correlation value.

Target	**N_f**	**E_γ range ΔE [MeV]**	**$\rho(I_\gamma/E_\gamma^3, S_{dp})$**		**$\rho_{max}(I_\gamma/E_\gamma^L, S_{dp})$**	**L(max)**
		[30]	[30]	[32]	[25]	[26]
F-19	6	2.3 – 5.5	-0.17			
Ne-21				*-0.28*		
Na-23	7	3.4 – 6.5	-0.06			
Mg-25	5	6.8 – 9.3	0.75		0.88	7.6
Al-27	14	2.7 – 7.8	0.78		0.93	0
Si-29	4	6.8 – 10.6	0.92			
P-31	5	5.2 – 7.9	0.84			
Cl-35	5	5.4 – 8.6	0.94		1.00	7.4
K-39	3	4.0 – 4.4	0.19			
Fe-56				*-0.08*		
Fe-57				*0.07*		
Co-59				*-0.12*		
Cu-63				*0.02*		
Ga-71				*-0.02*		

3 .2 The slope analysis

After the historical overview we turn our attention to the present PSF data which include a very comprehensive data base of M1 transitions. It seems, therefore, reasonable to exploit this data using the slope method (successful for E1) to address the average dependence of the reduced M1 strength and its behavior towards low E_γ energies.

The total M1 cross section strength σ(M1) has been deduced from equation (5) using data from Table 5

$$\sigma(M1) = \sigma(\gamma)_o \, \Sigma I_\gamma(M1) \qquad (5)$$

and the results are given in the third column of Table 7. Note that only for three targets is the σ(M1) cross section larger than 1 b (^{35}Cl, ^{45}Sc and ^{50}V) with the remaining nuclides having small cross sections in the milli-barns range. The column $\Delta E = E_\gamma^{min}$-$E_\gamma^{max}$ displays the width of the energy region with M1 transitions to indicate the quality of the data used for the derivation of the average slope E_γ dependence. For nuclides, such as for ^{39}K, ^{56}Fe, ^{59}Co, ^{62}Ni, and ^{65}Cu the narrow regions can seriously influence the accuracy of the slope estimate. In the column called <L> PSF the mean slope trend exponent is quoted, derived in the standard E_γ^{-3} dipole data reduction. The important conclusion is that all values have a negative sign what reflects the increasing M1 average strength with the decreasing gamma-ray energy E_γ.

Table 7 The fraction of the thermal cross section for M1 decay σ(M1) for A < 70 nuclides. The last four columns give the parameters for the slope analysis and its results. The last column shows the results from the (n,g)(dp) analysis from Ref. [25].

<L> - the exponent L of the power E_γ trend line derived from the slope of the PSF data
<<L>> - the derived E_γ exponent of the "theoretical" energy dependence of the initial I_γ data
$E\gamma^{min}$-$E\gamma^{max}$ – <value> a single M1 transition

Target	$\sigma(\gamma)_o$	σ(M1)	$E\gamma^{min}$-$E\gamma^{max}$	<L>	$<E\gamma^L>$	ρ
	[b]	[b]	< MeV>	PSF	<<L>>	nmax
						[25]
F-19	0.0095	0.0038	0.3 – 6.6	-1.80	1.2	
Na-23	0.525	0.39	0.7 – 6.5	-2.61	0.39	
Mg-24	0.0538	0.0029	2.2 – 6.7	-2.31	0.69	
Mg-25	0.199	0.14	3.9 – 11.1	-1.35	1.65	7.6
Mg-26	0.0374	0.0072	1.0 – 5.5	-1.48	1.52	
Al-27	0.231	0.12	0.4 – 7.8	-3.08	-0.08	0
Si-28	0.177	0.0175	1.6 – 8.5	-2.09	0.91	
Si-29	0.119	0.029	4.0 – 10.6	-3.19	-0.19	
P-31	0.166	0.059	1.1 – 7.9	-2.78	0.22	
S-32	0.518	0.036	2.0 – 8.6	-2.16	0.84	
Cl-35	43.6	19.45	2.0 – 8.6	-1.21	1.79	7.4
Cl-37	0.433	0.031	<4.2>			
K-39	2.1	0.29	3.9 – 5.5	-2.46	0.54	
Ca-40	0.41	0.017	3.4 – 6.4	-4.18	-1.14	
Sc-45	27.2	10.01	3.4 – 8.6	0.29	2.71	
Ti-48	8.32	0.067	2.7 – 8.6	-1.98	1.02	
V-50	45	1.53	<5.3>			
V-51	4.94	0.17	2.3 – 5.6	-1.36	1.64	
Fe-56	2.59	0.038	2.4 – 5.3	-1.96	1.04	
Co-59	37.18	0.669	2.7 – 5.1	-4.68	-1.68	
Ni-58	4.39	0.079	<7.2>			
Ni-60	2.45	0.042	3.6 – 7.2	-5.35	-2.35	
Ni-62	14.9	0.358	3.1 – 3.6	-0.27	2.73	
Cu-63	4.50	0.090	3.5 – 6.6	-3.75	-0.75	
Cu-65	2.17	0.186	2.5 – 4.9	-2.29	0.71	
Zn-64	0.731	0.039	3.6 – 6.1	-4.15	-1.15	
Zn-67	7.5	0.6	1.9 – 7.5	-6.57	-3.57	

The semi-direct M1 capture [30] is significant only for targets with $25 \leq A \leq 35$, following the occupation of the s- and d- orbits [32], and this probably explains the enhancement of ^{28}Al and ^{32}P nuclides. A very strong enhancement for ^{24}Na, which has a zero (nγ)(dp) correlation, presents a problem. In the ^{35}Cl case capture resonances strongly contribute to the cross section and the statistical behavior may than dominate, however, the strong (nγ)(dp) correlation is then a problem. The remaining three nuclides ^{40}K, ^{46}Sc and ^{52}V show no (nγ)(dp) correlation and semi-direct process enhancement is very unlikely. ^{46}Sc is the most peculiar case, the strong presence of the resonant

capture and the almost equal E1 and M1 strength presents a major question to solve. So far there is no consistent picture of the M1 enhancement and shape behavior from the earlier studies.

The slope analysis, however, provided results which do not support previous conclusions, such as the faster E_γ dependence of the L reduction factor from Ref. [25]. The expected faster decrease was based on the assumption that the spin-flip resonance is the dominant source of the M1 decay bellow the neutron binding energy. The presence of other collective excitations (e.g. the scissors resonance) at lower energies may explain this disagreement. The <<L>> column in Table 7 has values between -3 to +3 with a mean value of 0.34. Such result indicates that the PSF trend dependence on E_γ is increasing with decreasing E_γ as shown in Fig. 22, demonstrating the systematic increase of the M1 strength as E_γ goes to zero. This is a very relevant result, because from the other average resonance experiments (DRC, B and Sc filters) due to experimental limitations there are no primary PSF data smaller than 4 MeV available.

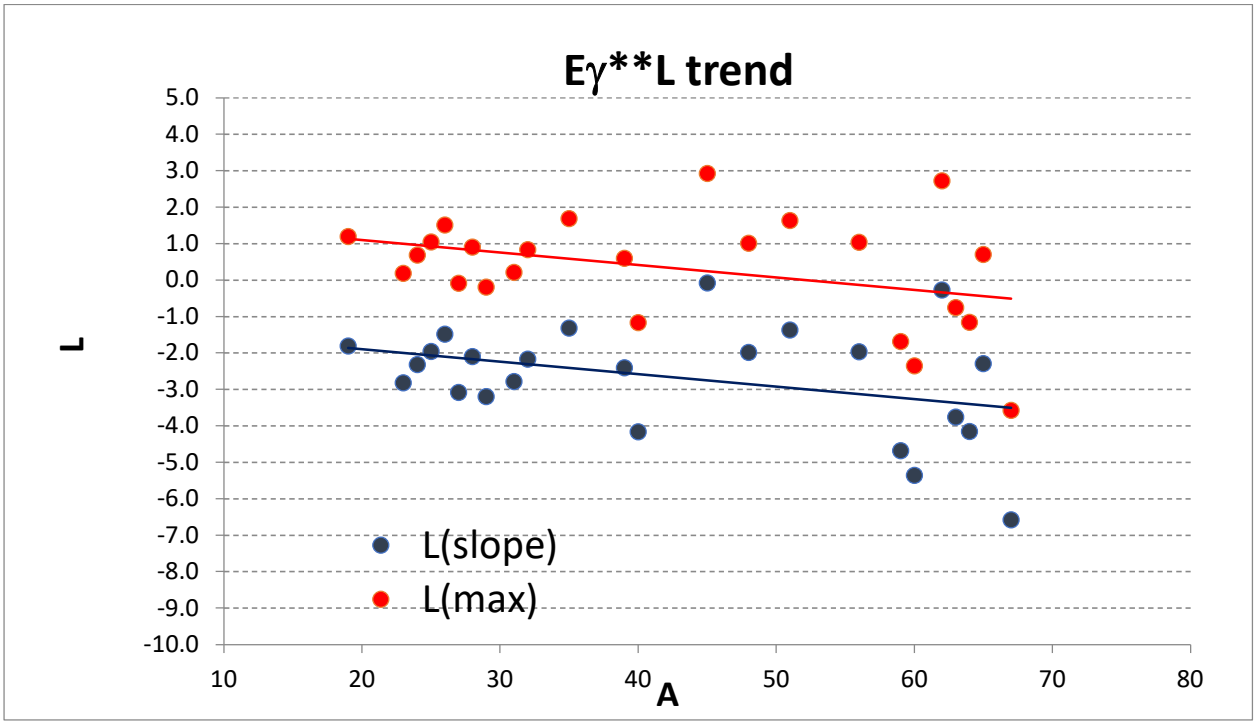

Fig. 22 *The distribution of the exponent L from the slope analysis of the PSF data and the corresponding L(max) of the theoretical E_γ shape dependence from the L(slope) = L(max) – 3 equation*

3.3 The comparison of the M1 strength with the D1M + QRPQ calculations

Contrary to the case of E1 radiation, where several validation options are available, such as comparison between the DRC and ARC data or comparison with the DRC systematics and finally against the theoretical QRPQ predictions (see Ref. [2]); the situation for M1radiation is different. The limited amount of M1 data makes the DRC comparison less accurate and the M1 DRC

systematics is too crude to use. This all makes the comparison against the theoretical D1M + QRPA calculations rather important both in assessing the shape and absolute values.

The systematical increase of the experimental M1 strength with E_γ - > 0 lends support for the majority of nuclides to the shape predicted by the D1M + QRPA calculations. However, the PSF data often show a strong enhancement of the M1 strength (see Fig. 2) above the calculated predictions and it seems reasonable to discuss the data in detail. We shall disregard discussions of nuclides with a small amount of M1 data points and targets with A > 70 and discuss only nuclides with sufficiently wide energy window with an adequate number of data points. The considered nuclides can be categorized into three groups:

1. <u>THC data in a disagreement with the D1M + QRPA M1-calculations at low E_γ</u>

The situation where there is a strong M1 strength enhancement against the theory, with a solid prediction of the slope shape (reasonably narrow dispersion of M1 data). The main examples are ^{24}Na, ^{28}Al and ^{32}P, all nuclides with a sufficient number of M1 transitions in a broad energy window down to E_γ ~1 MeV. The major enhancement takes place in the E_γ region between 0 and 5 MeV, well below the spin-flip resonance. This situation is comparable with a similar effect found for E1 transitions where non-statistical processes are present.

A comment on the ^{24}Na data: there is a large normalization uncertainty due to the missing evaluated $<\Gamma\gamma>$ value in Ref. [15]. Usually the $<\Gamma\gamma>$ is evaluated from the contributing resonances and in the ^{23}Na case only from positive resonances because the thermal cross section $\sigma(\gamma)$ = 0.525 b is 98% contributed by only $\sigma(+)$ and $\sigma(-)$. The resonance closest to the thermal capture state is at E_n = 2 keV with Γ_γ = 0.34 eV. The mean value of the four lowest s-wave resonances, spread up to 300 keV, is $<\Gamma\gamma>$ = 0.81 eV and this value was finally used in the PSF processing. This case shows how the accuracy of the PSF value seriously depends on the accuracy of the average $<\Gamma_\gamma>$ width. For studied nuclides (see Table 10) in this study the $<d\Gamma_\gamma>$values were spread from 0.07 up to 0.6 with a mean value of 0.29. Another important parameter, the spacing Do, is more accurate and the average uncertainty is 10%. The impact of this sensitivity of the PSF absolute values is demonstrated in Fig. 23, where the PSF data are compared with the theoretical predictions for two of the above discussed values of $<\Gamma\gamma>$ = 0.34 and 0.81 eV.

The E1 strength for ^{24}Na is in a reasonable agreement with the prediction; but the huge dispersion over more than 2 decades is suspicious. The M1 strength manifests a clear increase with decreasing E_γ, slightly underestimates the predicted curve between 4 -6 MeV near the spin -flip region but below 4 MeV starts to significantly overestimate the theory. The missing (ng)(dp) correlation indicates that no non-statistical effect is to be expected, which may be the reason of smaller M1 enhancement compared to other nuclides as e.g ^{28}Al.

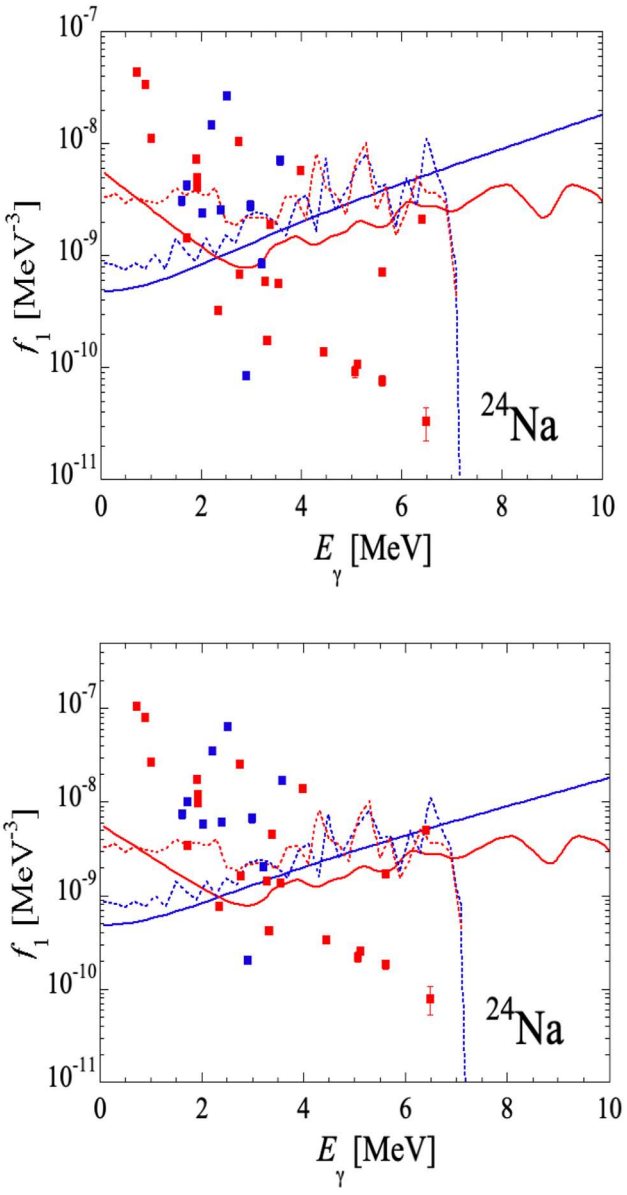

Fig. 23 *Comparison of two PSF evaluations of ^{24}Na with <Γγ> = 0.34 (left panel) and 0.81 eV (right panel) values to demonstrate the PSF sensitivity to the <Γγ> uncertainty. The full curves are the results of the D1M + QRPA calculations and the dotted curves originate from the shell model calculations [3]. The blue and red color is for E1 and M1 multipolarities. Note a remarkable agreement between the D1M + QRPA and SM calculations*

The ^{28}Al nuclide is one of the most instructive examples for the behavior of the M1 strength. It may therefore function as a model case to test the theoretical model. The data agree with the prediction of both D1M + QRPA and SM calculations down to $E_\gamma \pm 3$ MeV and starts to increase faster to zero energy. This deviation is present in all the studied nuclides and the shape probably varies with the size of the contributions (non-statistical?) at very low E_γ energies. The strong (nγ)(dp) correlation of $\rho = 0.78$, supports the semi-direct process [29] as the most likely. The accuracy of the ^{28}Al evaluation is rather high, the relevant input parameters have small errors [$<\Gamma_\gamma> = 1.61(36)$ and $D_o = 53(7)$] that gives the average accuracy of the PSF trend a value of about 30%.

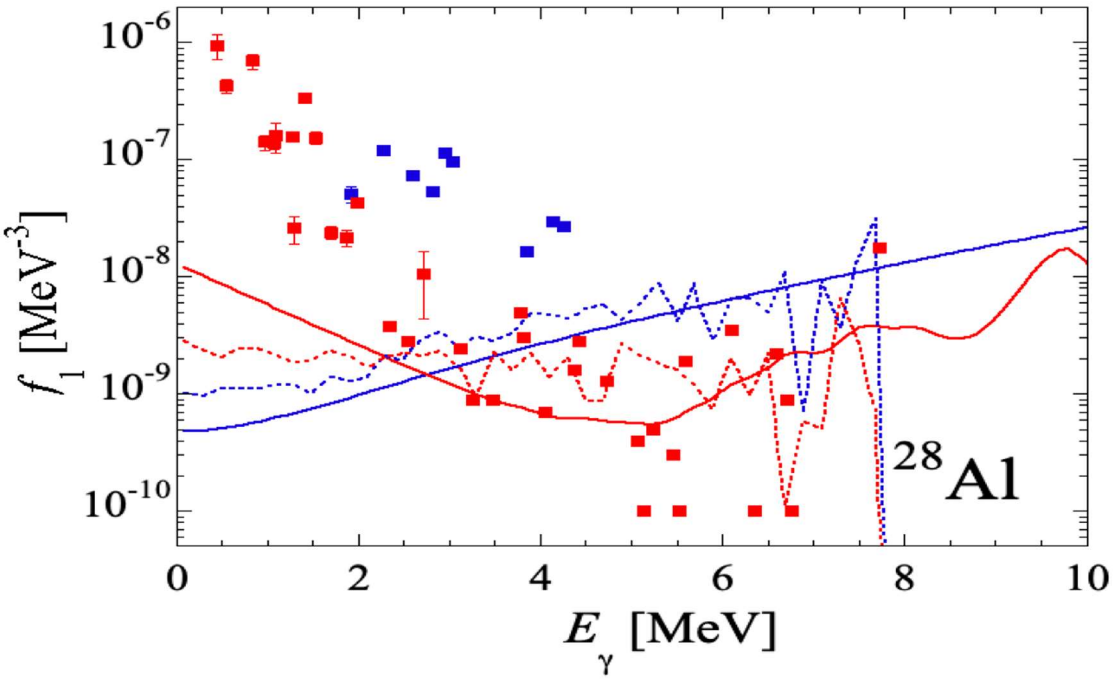

Fig. 24 *Comparison of the PSF evaluation of ^{28}Al with theoretical predictions. The M1 data are in a good agreement with predictions down to E_γ = 4MeV and from this energy a systematic increase of the strength takes place. The formatting of curves and colors is the same as in Fig. 23*

The ^{32}P nucleus is a similar case to ^{28}Al, again with a significant correlation $\rho = 0.84$ and the M1 data satisfactory fit the D1M + QRPA calculation above 3 MeV but start to be enhanced for $E_\gamma < 3$ MeV. The accuracy of the PSF data is slightly inferior to the Al data, the bound state contribution is fully responsible for the thermal cross section and $\langle\Gamma_\gamma\rangle = 2$ eV was estimated from the BW cross section fit as a function of E_n with no error. But the PSF M1 data of these two nuclides look similar, which supports the idea that they represent the M1 strength shape in case where the low energy data are influenced by non-statistical effects.

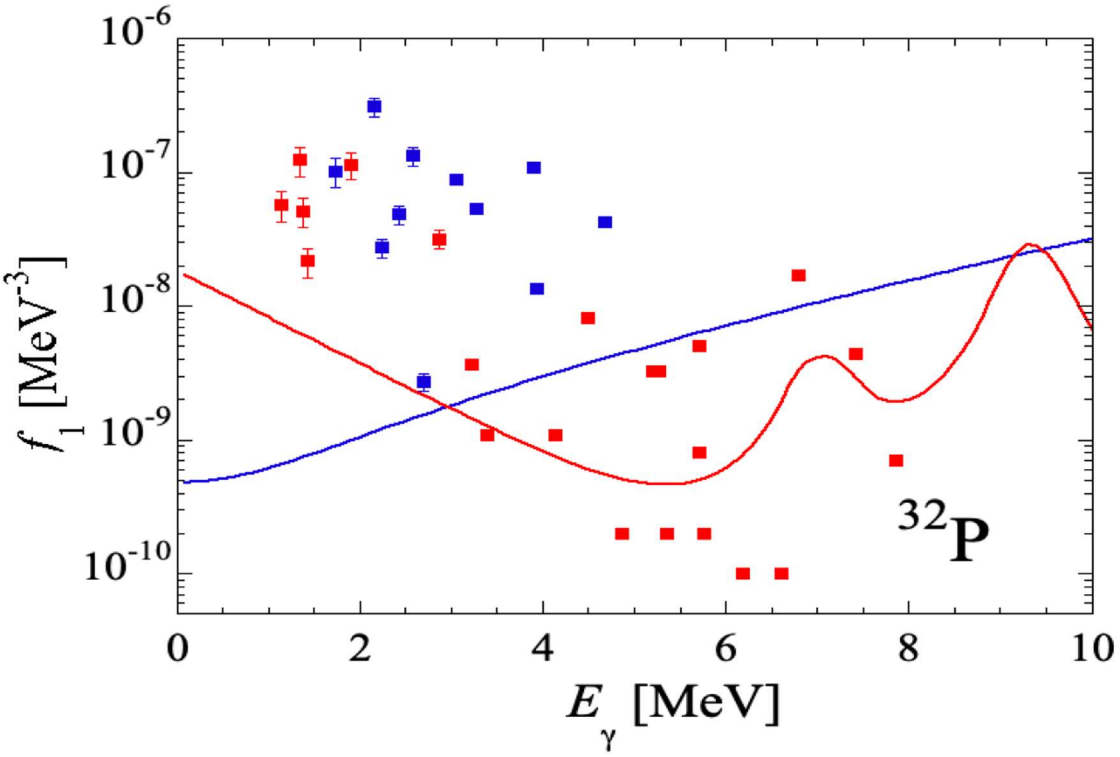

Fig. 25 *Comparison of the PSF evaluation of ^{32}P with the theoretical prediction. The M1 data are in a good agreement with predictions down to E_γ = 3 – 4 MeV and from this energy a systematic increase of the strength is evident. The formatting of curves and colors is the same as in Fig. 23*

2. <u>THC results in good agreement with the D1M + QRPA calculations:</u> Typical examples are ^{36}Cl and ^{57}Fe.

The thermal cross section of 43.6 b for the ^{35}Cl(n,γ)^{36}Cl reaction is formed by a strong negative resonance close to the Q-value and a statistical nature is expected. This may explain the good agreement with the D1M + QRPA calculation which follows the CN model. The reasonable accuracy of $\langle\Gamma_\gamma\rangle$ and Do parameters guarantee that the PSF data trend is rather accurate. As mentioned earlier, the non-statistical behavior of M1 is found in the ^{35}Cl target [29]. In the capture from two neighboring s- and p-wave resonances the M1 strengths were found to be correlated to the E1 intensities from thermal capture and to agree with SP estimates, which suggests the presence of non-statistical nature via the doorway states as stated in Ref. [28]. The conclusion is that this nucleus has one of the best agreements with the D1M + QRPA theory (see Fig.26).

The ^{56}Fe(n,γ)^{57}Fe reaction thermal cross of 2.59 b is fully contributed by a bound state and therefore is certainly of a resonant nature. The accuracy of $\langle\Gamma_\gamma\rangle$ is about 50%, but the agreement of M1 strength between 2 – 5 MeV is remarkably good. This demonstrates that the resonance process in this energy region is well reproduced by the D1M + QRPA calculation as shown in Fig. 27.

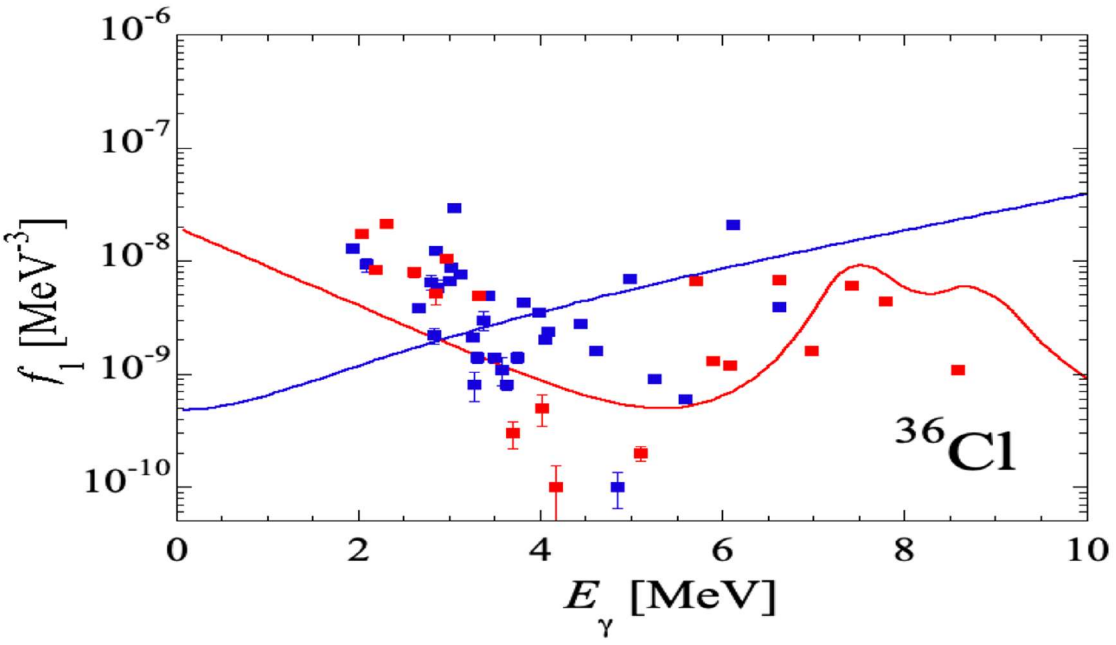

Fig. 26 *Comparison of the PSF evaluation of ^{36}Cl with the theoretical prediction. The M1 data are in a good agreement with the prediction almost to E_γ = 3 MeV. The formatting of curves and colors is the same as in Fig. 23*

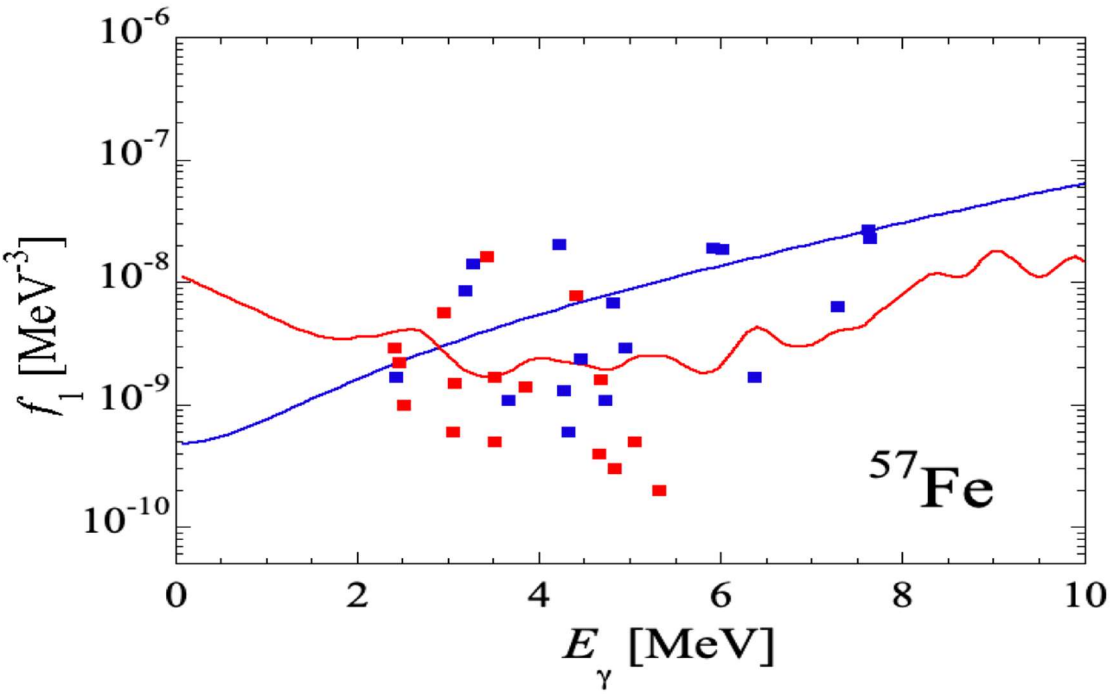

Fig. 27 *Comparison of the PSF evaluation of ^{57}Fe with the theoretical prediction. The M1 data are in a good agreement with the prediction in the region E_γ = 2 - 5 MeV. The formatting of curves and colors is the same as in Fig. 23*

3. THC data in serious disagreement with the D1M + QRPA calculations: typical examples are ^{40}K and ^{46}Sc and partially ^{52}V.

In this case there is a M1 enhancement with a broad dispersion of data points in a narrow energy region (Fig. 29). This is an example where the uncertainty of the spin/parity assignment may the source of decreased accuracy. In this case it concerns the E1 data, where a number of points were assigned as having E1 multipolarity based on the parity assignment in the ENSDF file, shown as (π) in brackets. If we omit these data points, then the slope of E1 is changed as shown in Fig. 30. The thermal cross section is seen to be entirely due to the bound state component. However, the reason for enhancement of the M1 strength remain unanswered and missing (ng)(dp) correlation excludes any non-statistical doorway state explanation.

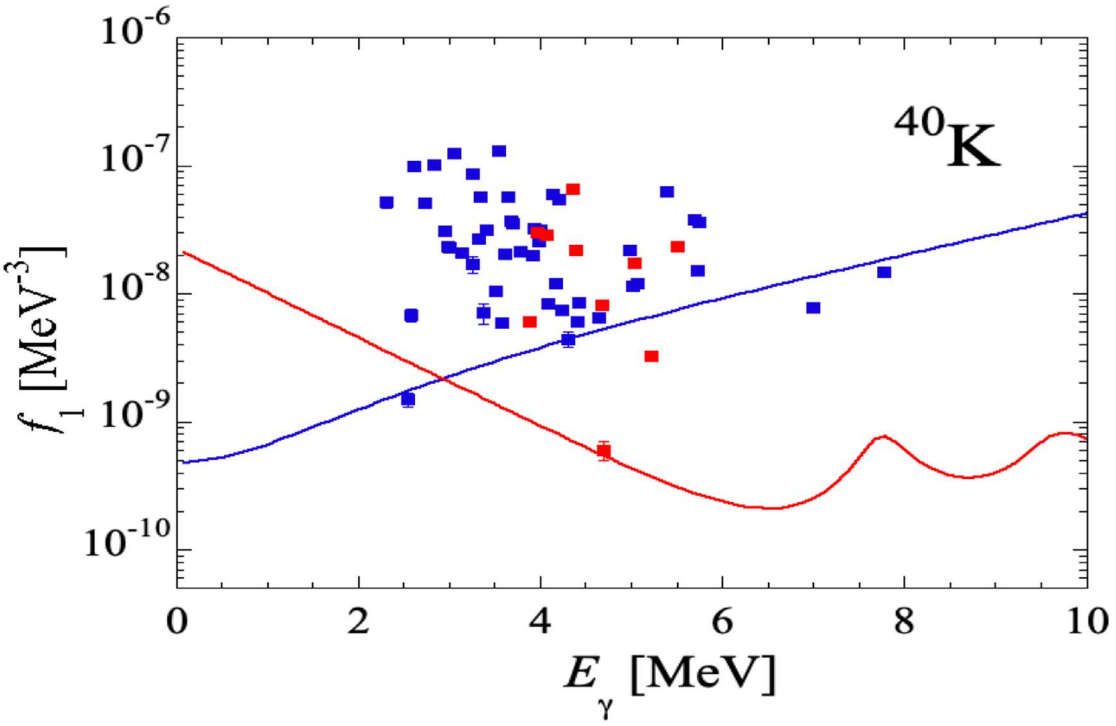

Fig. 29 *Comparison of the PSF evaluation of ^{40}K with the theoretical prediction. The M1 data are heavily enhanced against the prediction in the region E_γ = 4 - 5 MeV. The formatting of curves and colors is the same as in Fig. 23*

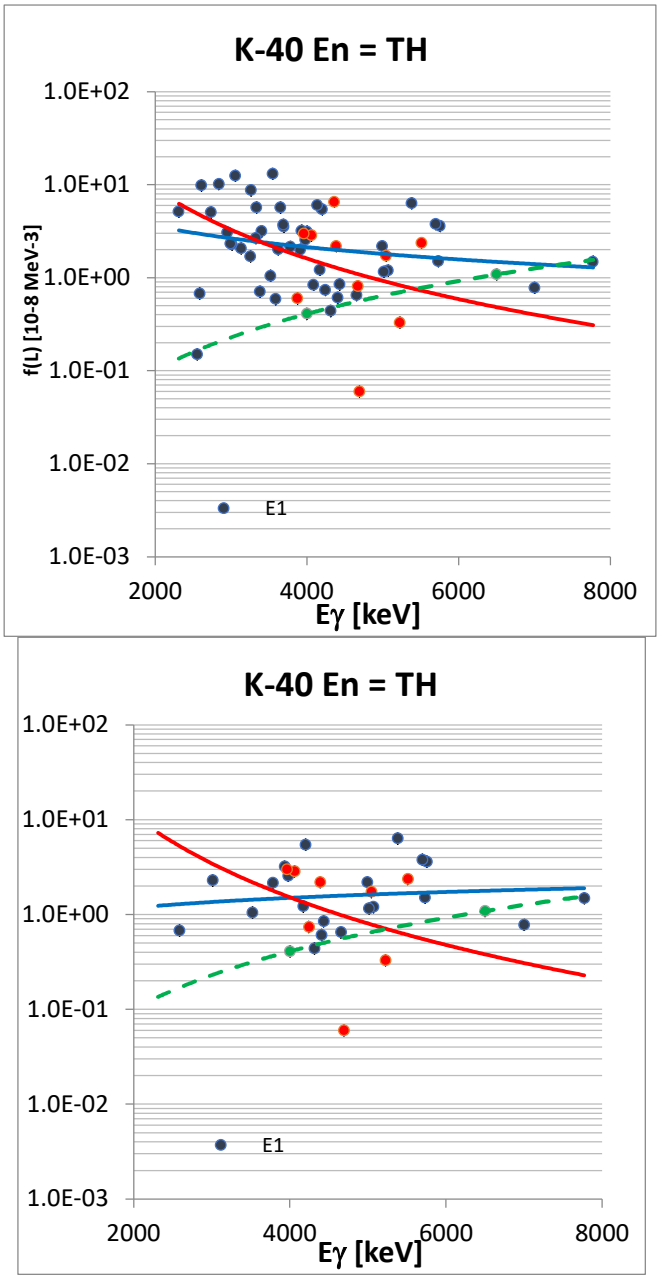

Fig. 30 *The influence of the data selection based on the ENDSF criteria for strong and weak arguments of the parity. The left-hand plot shows all E1 transitions with both assignments (strong and weak - π in brackets) and in the right-hand plot only transitions are plotted to states with the strong parity assignment. Note the difference in the slope trend of E1 data.*

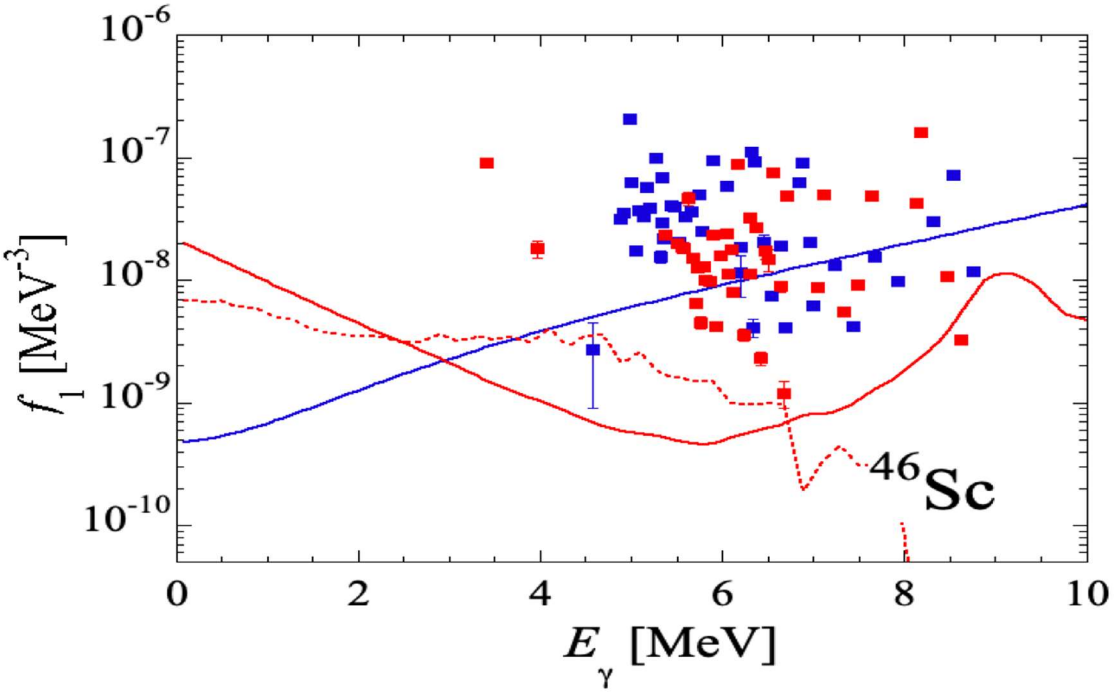

Fig. 31 *Comparison of the PSF evaluation of ^{46}Sc with the theoretical prediction. The M1 data are severely enhanced against the prediction in the region E_γ = 4 - 7 MeV. The formatting of curves and colors is the same as in Fig. 23*

In the ^{45}Sc(n,γ)^{46}Sc reaction the E1 strength agrees reasonably with the predicted curve but the M1 data are well above and surprisingly of an equal strength with the E1 radiation. The absolute calibration due the $\langle\Gamma_\gamma\rangle$ value with 50 % error creates a common uncertainty for both multipolarities. This is a rather puzzling effect in the capture reaction at about 6-7 MeV, especially in the view that the thermal cross section of ^{45}Sc is due to the bound region with two resonances with $J_i = 3^-$ and 4^-. However, the polarized neutrons/target experiment yields the average spin admixture of $\langle\alpha\rangle = 0.05$, with the absolute preference of the spin $J_i = 3^-$ [1,33,34]. Ref. [33] suggests that the M1 data have a faster dependence than E_γ^3 but with no justification given.

The situation for the ^{51}V(n,γ)^{52}V reaction is different. Because both multipolarities are enhanced compared to the theoretical curves in the whole region, it may be an absolute normalization problem. The relevant input parameters, $d\Gamma_\gamma$ has no uncertainty and dD_o = 7% is rather accurate. In order to explain the enhancement, the $\langle\Gamma_\gamma\rangle$ value should be smaller by factor of three to four, which is very unlikely in the view of Γ_γ values of the five lowest resonances. The thermal cross section is constructed from about 4 resonances and the spin admixture $\langle\alpha\rangle$ = 0.77 and 0.23 for $J_i = 3^-$ and 4^-, respectively.

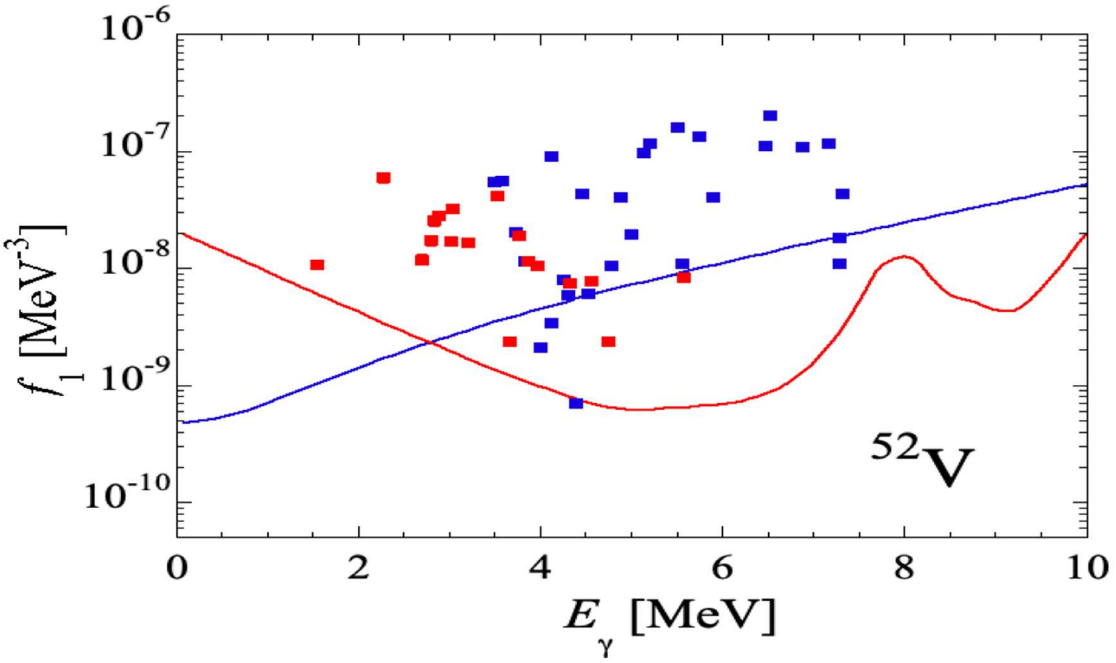

Fig. 31 *Comparison of the PSF evaluation of ^{52}V with the theoretical prediction. The M1 data overestimate the prediction in the region E_γ = 2 - 5 MeV by four to five having a good trend slope. The formatting of curves and colors is the same as in Fig. 23*

3.4 Discussion and conclusions

The M1 thermal capture behavior with A < 70 have been reviewed using the earlier results and extended with the recent PSF data [1]. The PSF data have been treated in a similar manner as the E1 data to identify the E_γ dependence which may give information of the reaction processes involved in the (3s –> 2s,1d) final state configurations. There is very little known about the reaction models except for the statistical CNM. A rather limited non-statistical doorway-state mechanism was proposed for a rather restricted mass region.

The recent conclusions and observations can be summarized as follows:

1. M1 transitions are a minor decay process accounting for about 6 % of the total strength in thermal capture. This conclusion is based on the comparison of the total transition strengths, given as ΣI_γ(E1) and ΣI_γ(M1) for primary transitions.

2. This theoretical modelling assumes collective M1 excitations, as spin-flip or scissors and up bend components, obeying features of the CNM. A limited amount of the reduced (n,γ) (n,d) correlations (24 < A < 32) and the corresponding non-statistical modelling certainly do not justify applying this approach for the whole mass region.

3. A similar analysis, as was done for the thermal PSF E1 data, where the trend slope of the PSF data analysis was used, has been applied. This procedure gives the average trend slope dependence on the energy E_γ and this forms relevant information for the

theoretical prediction and its average strength.

4. The response of the M1 experimental strength compared to the D1M + QRPA calculations gives only one solid result, namely that the strength starts from the energy of the spin-flip resonance to increase as the energy E_γ --> 0.

5. The comparison of the absolute strength values is controversial. There are nuclides with a clear enhancement but also cases with a good agreement. The comparison is complicated by the fact that for many nuclides the E1 and M1 strengths for $E_\gamma < 5$ MeV often becomes equal which increases the chance of multipolarity misinterpretation.

6. A very speculative conclusion suggests that reactions with a strong resonance character and large $\sigma(\gamma)$ are in a better agreement compared to low cross section targets. Another speculative observation concerns the region just below the spin-flip resonance energy (4-6 MeV) which may be described better for the deformed than for the spherical nuclei.

4. General conclusions and future perspectives

The Photon Strength Function (PSF) behavior has been studied in a comprehensive effort using different types of neutron capture reaction. Among them are the average resonance capture using different beam filters, such as B, Sc and Fe, (the ARC data) and from the capture in the discrete resonances that are then averaged numerically (DRC data). Final results have been documented in several papers [1,2,34] and the data base stored in ATLAS_PSF data base at NDS [35]. This library forms a solid data base of PSF values for nuclides with masses above A > 70- 80 and the gamma-ray energies $E_\gamma > 4$ MeV. A systematic describing the E1 data was produced and this shows good agreement with the theoretical calculations (using the D1M+QRPA theory) as shown in Fig. 32 taken from Ref. [2]. The agreement is remarkably good down to a mass of A ~ 50 where a discrepancy with the experimental DRC data points becomes large. The accuracy of the <f(E1)> values in that region becomes smaller because of limited number of resonances which decreases the averaging power and eventually enables the non-statistical effects to influence the data.

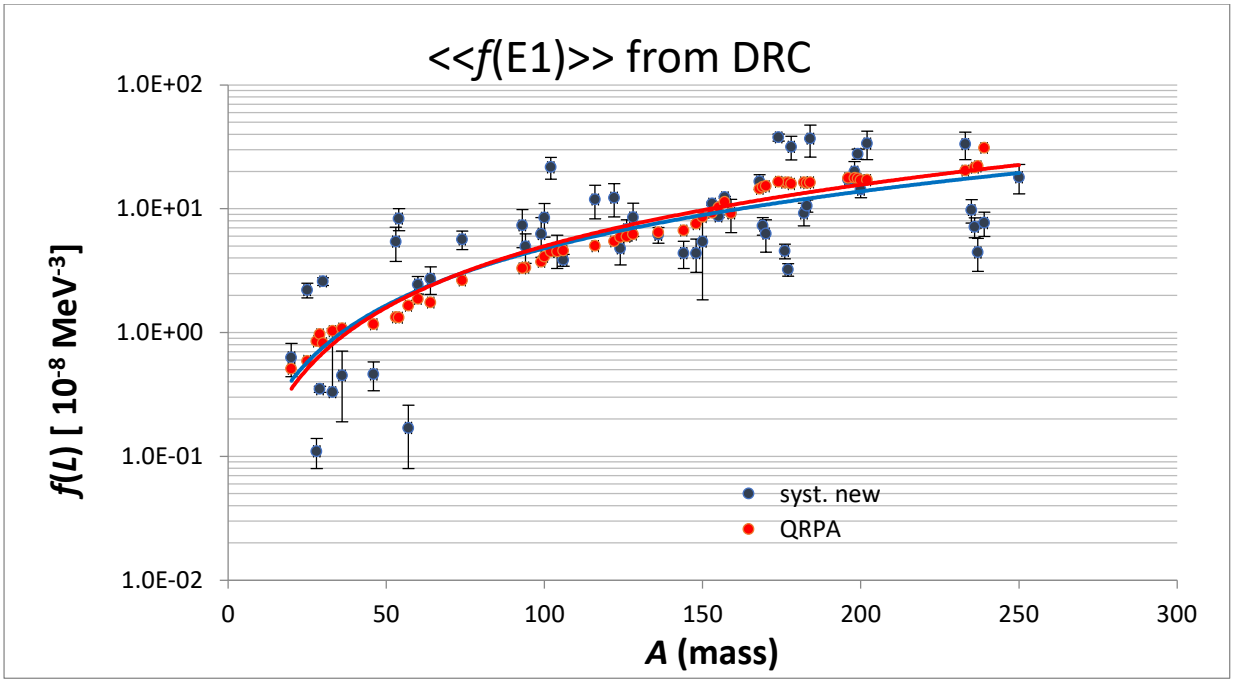

Fig. 32 *Comparison between the E1 experimental DRC PSF binned in the 6.5±0.5MeV range and D1M+QRPA predictions in the same energy window. The outliers at A about 100 and 180 are discussed in detail in Ref. [2].*

Less successful is the comparison for the M1 systematics as displayed in Fig. 33 (again from Ref. [2]) in which the M1 systematics begins at A ~ 100 to be larger than the D1M+QRPA prediction and especially below A = 50 the difference is rather significant.

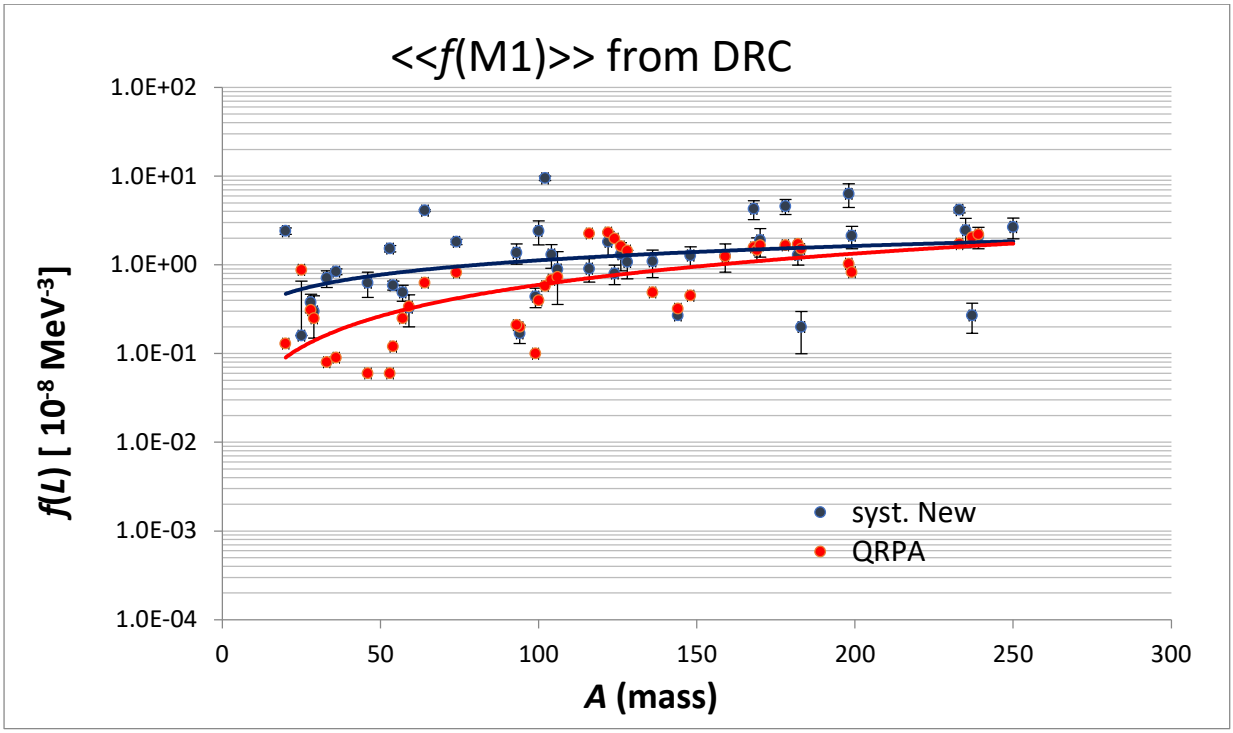

Fig. 33 *Comparison between the M1 experimental DRC PSF binned in the 6.5±0.5MeV range and D1M+QRPA predictions in the same energy window*

These differences turned attention to thermal capture (THC), because this reaction may help to clarify some of the above problems. The thermal capture spectra have a much better statistical accuracy than the ARC or DRC spectra and uniquely this applies to the whole energy range $0 < E_\gamma < B_n$. Because of a low density of final states for low mass targets many of the low energy primary transitions can be detected exactly in the range which is missing in the average spectra. This range lies for $E_\gamma < 4$ MeV, usually below the detection sensitivity limit for DRC or ARC measurements. Another special feature of THC is that the capture state cross section represents the state formed by the tails of distant levels, especially for low mass targets with a very low cross section value, and the non-statistical direct capture mechanism may influence especially the E1 strength. For higher neutron energies these processes are dominated by the statistical compound nucleus mechanism.

A final advantage of the THC data is the improvement of the light target completeness. The mass region with solid ARC and DRC data starts at A = 76 and the THC data which allows extension below this mass are shown in Table 8. The first three columns indicate the selected DRC and ARC data and the last column the sources of the THC data.

.

Table 8 Listing of the PSF data included in the ATLAS_XXX data base and the THC data available to be added. The inputs denoted with (x) is not included due to the insufficient averaging. The column with #l_n displays the number and angular momentum (l_n) of resonances included in the DRC data.

Product nuclide	**ARC**	**DRC**	**# l_n resonances**	**THC**
F-20		x	2 p	x
Na-24				x
Mg-25		x	1 p ;1 d	x
Mg-26				x
Mg-27				x
Al-28		x	1 s;1 p	x
Si-29		x	1 d	
Si-30		x		
P-32				x
S-33		x		
Cl-36		x	1 p	x
Cl-38			1 p	x
K-40				x
Ca-41				x
Sc-46	(x)	x	2 s	x
Ti-49	(x)			x
V-51				x
V-52				x

Cr-53		x	1 p	
Cr-54		x	8s; 5p	
Fe-57		x	1 p	x
Fe-58				x
Fe-59		x	2 p	
Co-60		x	1 s	x
Ni-59				x
Ni-61				x
Ni-63				x
Cu-64	(x)	x	3 s	x
Cu-66	(x)			x
Zn-68				x
Ge-74		x	6 s	
As-76	x			

The overview of discrete resonances in the DRC processing (see Table 8) shows that for majority of nuclides only one or two s-, p- and even d- wave resonances are used. This situation, which has often been followed where there are only a small number of transitions, gives a rather limited averaging power and the resulted PSF values are associated with large uncertainties. Many of these PSF data suggest the presence of non-statistical processes (e.g. M1 stronger than E1) which may vary with the l_n value of the initial state. Only three nuclides have sufficiently large averaging, namely the ^{54}Cr, ^{64}Cu and ^{74}Ge nuclides for a valid comparison with THC data.

The thermal data, with their superior gamma-ray spectra quality, certainly may give additional and relevant information on the PSF behavior. One example is shown in Fig. 34 in which the difference of the DRC and THC experimental response is shown for the ^{64}Cu product nucleus. This comparison demonstrates how the DRC data cover only a fraction of the total E_γ range, just below the neutron binding energy.

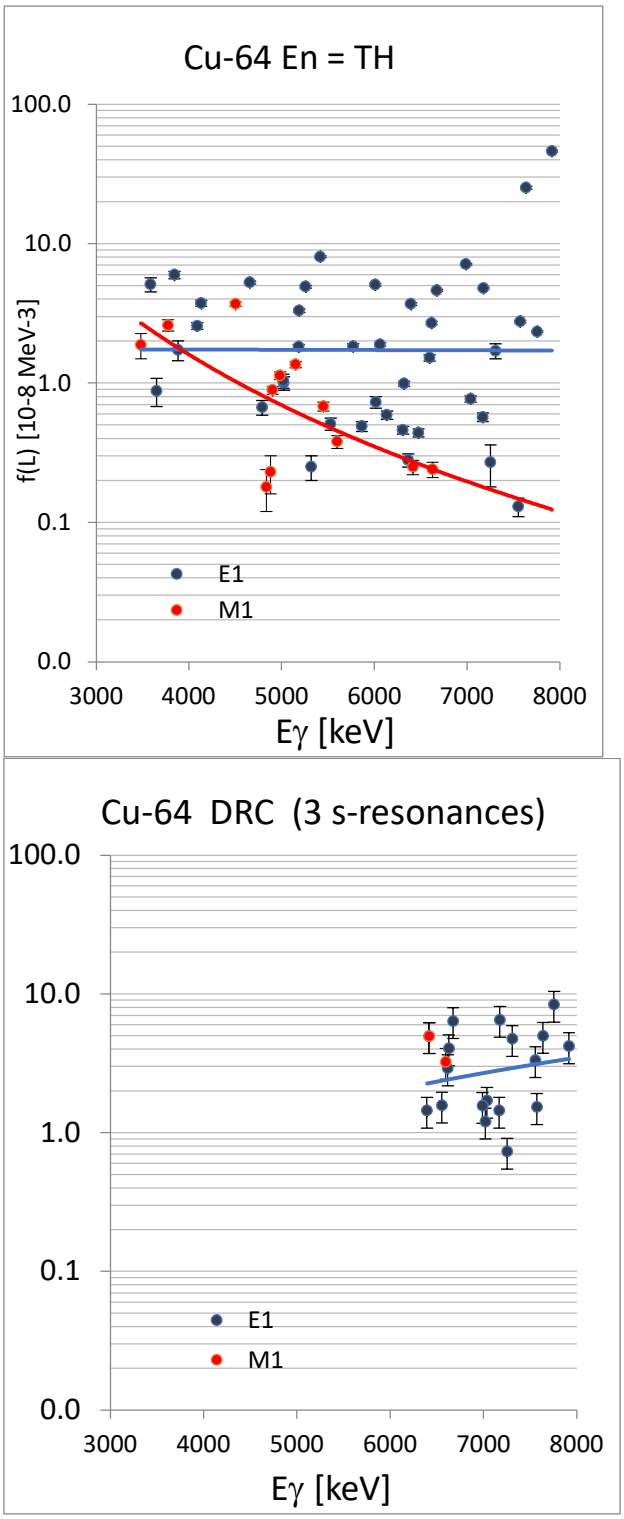

Fig. 34 *The $^{63}Cu(n,\gamma)^{64}Cu$ reaction THC and DRC PSF results. The plotted curves are the unweighted power trend lines. Note the size of the energy region addressed by the DRC experiment compared to thermal capture.*

Comparison of DRC and THC data from Table 8 is graphically shown in Fig. 35 in a combined plot of E1 and M1 transitions. In these plots the average <<f(L)>> values, binned in the E_γ = 6.5 $\pm$ 0.5 MeV window, using data with at least two transitions, are plotted for targets with A < 100. The agreement of the two different data sets is rather good considering the very low

degree of averaging and serves as an internal validation of the THC data processing. The E1 strength trend from THC is slightly larger than the DRC data while for the M1 strength trends the situation opposite way. The combination of results from these two experiments increases our understanding of the PSF response in this mass region and challenges the theory to describe it.

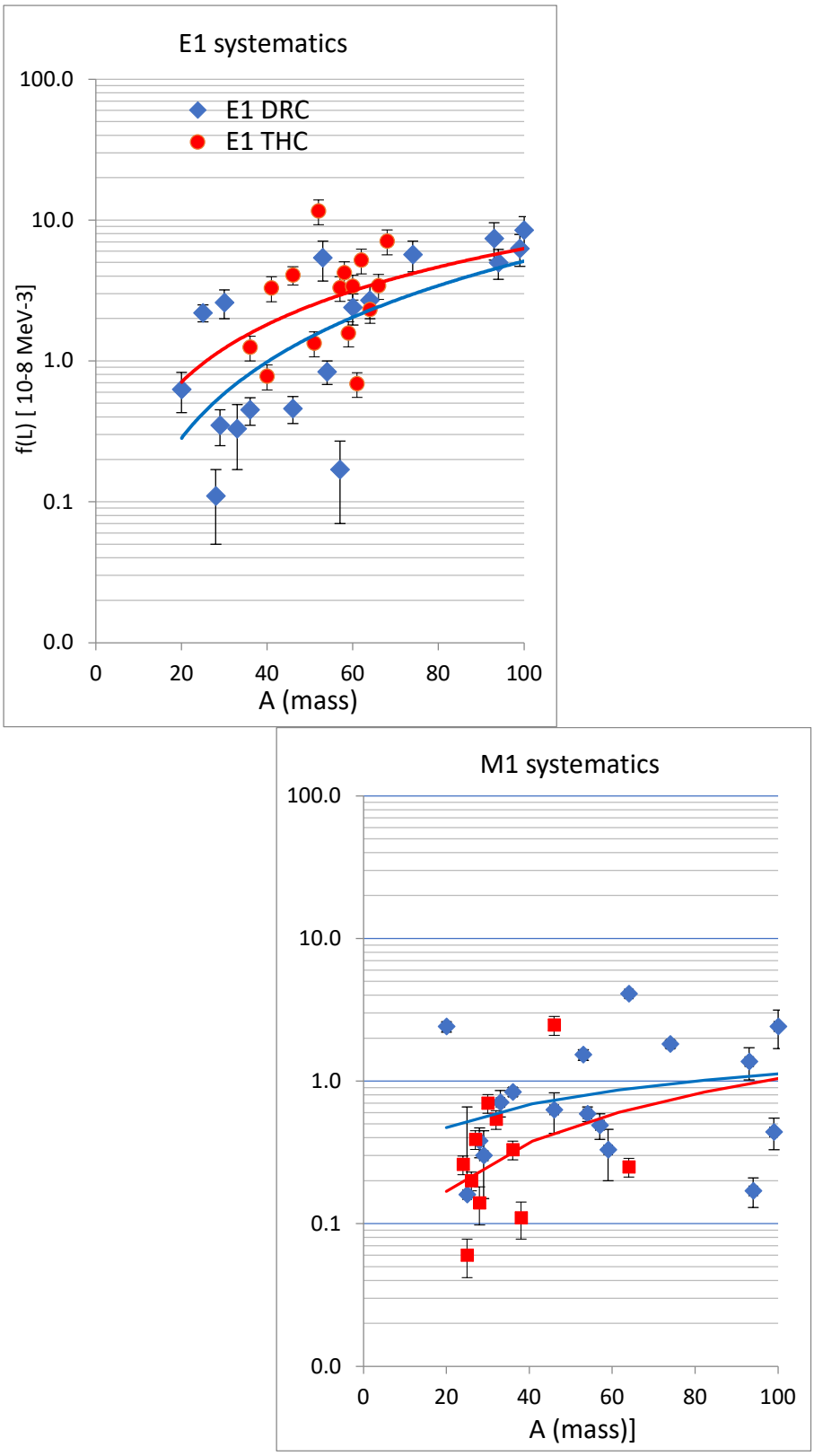

Fig. 35 The *<<f (E1>> and <<f(M1)>> data, binned within the 6 – 7 MeV energy window, plotted separately. The blue data points describe the DRC data while the red ones show the recent THC results. Note the concentration of E1(M1) data above (below) A ~ 40, respectively as a reflection of the availability of proper final states. Further note a slight increase of the THC E1 data by less than a factor of two compared to the DRC trend while for the M1 radiation the situation is opposite. The systematics <f(L)> curves remain practically unchanged for A > 100.*

The results of the robust study of the thermal capture PSF data from Ref. [1] and the present work are summarized in the following major conclusions and observations, primarily for targets with A < 70:

1. Different procedures for the absolute normalization of the PSF values have been tested in Ref. [1] and finally the standard procedure as for the DRC and ARC data have been adopted as a satisfactorily accurate and practical procedure in the view of all present uncertainties, such as the PT fluctuations or the spin admixture in the capture state.
2. The thermal capture data of 24+9 nuclides with masses 19 < A< 70 and 90 <A < 154, respectively, have been evaluated in the partial PSF data using the standard procedure. The partial transition strength has been processed using the pertinent parameters I_γ, $<\Gamma_\gamma>_o$ and D_o. No binning of the partial PSF data, as the approach of Firestone in Ref. [35], has been applied.
3. The main advantage of partial data is that the energy dependence of the slope can often be extracted, which serves as a signature of the reaction process.
4. The major source of the processing uncertainty is in the use of the average width $<\Gamma_\gamma>_o$ for absolute normalization. This value, evaluated in Ref. [25] from a large set of measured resonance parameters, is certainly a good parameter for the DRC and ARC data. However, the thermal capture state is a very specific state, formed either by tails, which interfere, of distant resonances or often of one strong nearby resonance and finally also from the potential capture (usually "poisoned" by the direct capture) meaning that the $<\Gamma_\gamma>_o$ value may not be the best choice. It seems, however, that this situation is rather rare and the PSF enhancement of both E1 and M1 strengths against the <f(L)> systematics or D1M+QRPA predictions serves as a warning.
5. The distribution of the E1 THC strength can be phenomenologically well understood as a combination of two processes, the non-statistical direct capture for targets with A < 40 and the responsibility for an enhancement over the statistical compound nucleus model. In the second process, the statistical model smoothly takes over around A > 50 and is also dominant in targets with a strong resonant nature of the thermal cross section (usually one single strong resonance). The theoretical approach is challenged to implement this situation in the PSF calculations for incident thermal neutron energies.
6. The distribution of the M1 strength is less well understood. The theoretical description of the possible M1 non-statistical processes is rather scarce and incomplete. The strength increasing with E_γ --> 0 is well described by the D1M+QRPA calculations but the THC PSF M1 data are often larger than these predictions and no systematic explanation has been established.
7. The future THC work should concentrate on the M1 behavior and on the other mass region where nonstatistical effects are expected.
8. In the general data base of THC, DRC and ARC data files, those targets indicated as E1 and M1 outliers compared to the systematics or the theoretical predictions, should be reviewed, particularly regarding the absolute normalization.

Acknowledgments

My thanks go to Stephane Goriely, who supported the idea to look further at the thermal neutron capture data for PSF applications and providing for all the D1M+QRPA plots. Many comments of Vivian Dimtriou concerning the manuscript are highly appreciated. Last but not least, I thank Robin Forrest for our continuing contact, both in the professional and friendship sphere, as the always open “help desk”.

The IAEA NDS and its head Arjan Koning are thanked as a supporting institution.

References

[1] J. Kopecky, "*Photon Strength Functions in Thermal Capture"* INDC(NDS)-0799, February 2020

[2] J. Kopecky and S. Goriely. "*Strength Functions derived from the Discrete and Average Resonance Capture"* INDC(NDS)-0790, July 2019

[3] S. Goriely and K. Sieja, priv. communication and S. Goriely et al., "*Reference Database for Photon Strength Functions*", Eur. Phys. J. A (2019) 55 17

[4] A.M. Lane and E. Lynn, Nucl. Phys. 17 (1961) 563, 586

[5] S.G. Mughabghab et al., Phys. Rev. Lett. 26 (1971) 11a18

[6] S.G. Mughabghab et al., Phys. Lett. 35B (1971) 469

[7] S.G. Mughabghab et al., Phys. Lett. 81B (1979) 93

[8] J. Honzatko et al., Czech.J.Phys. B30 (1980) 763

[9] S. Raman et al., in Neutron Capture Gamma-Ray Spectroscopy and Related Topics (Inst. of Physics, Bristol 1981) 357

[10] S.G. Mughabghab et al., Phys. Rev. 8C26 (1982) 2698

[11] S.G. Mughabghab et al., Phys. Rev. 81B (1979) 93

[12] R.F. Carlton et al., in Neutron Capture Gamma-Ray Spectroscopy and Related Topics (Inst. of Physics, Bristol 1981) 34

[13] R.L. Macklin et al., Phys. Rev. C32 (1985) 379

[14] S. Raman et al., Phys. Rev. C39 (1989) 1297

[15] S.F. Mughabghab "*Atlas of Neutron Resonances*" (Elsevier 2018)

[16] J. Kopecky and F. Stecher-Rasmussen, "*On the correlation between (d,p) and (n,γ) strength in the mass region A = 40-70",* Proc. Int. Conf. on Nuclear Structure Study with Neutrons, Budapest, July 31-August 5, 1972, p. 324.

[17] J. Kopecky et al. "*The (d,p) (n,γ) correlations in the mass range A = 24-80"*, Proc. Int. Conf. on Nuclear Physics, Munich, August 27-September 1, 1973, p. 523.

[18] A.M.J. Spits and J.A. Akkermans, Nucl. Phys. A215 (1973) 260

[19] J. Kopecky, "*Analysis of the Non-statistical Effects in the (n,γ) Reaction in the mass Region A = 40 – 70*", RCN report (1973), RCN-73-003

[20] J. Kopecky, "*Analysis of the Non-statistical Effects in the (n,g) Reaction in the mass Region A = 40 – 70*" RCN report (1973), RCN-73-094

[21] J. Kopecky and A.M.J. Spits, "*Some features of the correlation between the (d,p) and (n,g) reduced width*" RCN report (1974), RCN-74-055

[22] J. Kopecky and C. Plug, "*Tables of the (n,γ) (d,p) correlations in the 3s- region"* RCN Report (1975), RCN-75-005

[23] J. Kopecky, A.M.J. Spits and A.M. Lane, Phys. Lett. 49B (1974) 323

[24] J. Kopecky and A.M.J. Spits, "*Direct capture on the $^{37}Cl(n,\gamma)^{38}Cl$ reaction"*, Proc. Int. Conf. on The Interactions of Neutrons with Nuclei, Lowell, Massachusetts, U.S.A., July 6-9, 1976, (CONF- 60715-P2) p. 1285

[25] S. Mughabghab, "*Non-statistical effects in neutron capture*", Conf. III International School on Neutron Physics, Alusha (The Crimea) USSR, April 1978.

[26] S.Prussin et al., Phys. Rev. C16 (1977) 1001

[27] A. Bohr and B. Mottelson, "*Nuclear Structure Vol. II*", (Benjamin, London) 1975

[28] J. Kopecky, "*Anomalous M1-capture in mass region A=20-40"*, Proc. Int. Conf. on the Interactions of Neutrons with Nuclei, Lowell, Massachusetts, U.S.A., July 6-9, 1976, (CONF-760715-P2) p. 1285

[29] R.E. Chrien and J. Kopecky, Phys. Rev. Lett. 39 (1977) 911

[30] C.F. Clement, A.M. Lane and J. Kopecky, Phys. Lett. 71B (1977) 10
[31] J. Kopecky, "*Mass and energy dependence of radiative strength near neutron threshold*", Proc. Int. Conf. on Nuclear Physics, Berkeley, Cal., U.S.A., August 24-30, 1980, (North-Holland Publ. Comp., Amsterdam, 1981) p. 198 in Abstracts
[32] J. Kopecky, "*Nonstatistical features of M1 transitions near neutron threshold*", ibid, p. 209
[33] T.A.A. Tielens et al., Nucl. Phys. A 376 (1982) 421
[34] H.I. Liou et al., Nucl. Phys. A 337 (1980) 401
[35] R. Firestone in Eur. Phys. J. A (2019) 55 172

Nuclear Data Section
International Atomic Energy Agency
Vienna International Centre, P.O. Box 100
A-1400 Vienna, Austria

E-mail: nds.contact-point@iaea.org
Fax: (43-1) 26007
Telephone: (43-1) 2600 21725
Web: https://nds.iaea.org